# Parity violation in nd interactions

Jared Vanasse

Phys. Rev. C **86**, 014001 — Published 2 July 2012

DOI: 10.1103/PhysRevC.86.014001

# Parity Violation in $nd$ Interactions

Jared Vanasse*

Department of Physics-LGRT,

University of Massachusetts,

Amherst, MA 01003

(Dated: May 23, 2012)

## Abstract

We calculate the parity-violating amplitudes in the $nd$ interaction with pionless effective field theory to LO. Matching the parity-violating low energy constants to the DDH coefficients we make numerical predictions for parity-violating observables. In particular we give predictions for the spin rotation of a neutron on a deuteron target, and target and beam asymmetries in $nd$ scattering.

* jjvanass@physics.umass.edu

# I. Introduction

Hadronic parity-violation has been traditionally analyzed in terms of potential models; specifically the DDH model[1], which is a parity violating single meson exchange picture containing seven phenomenological constants. However, there exist well known discrepancies between experimental measurements and the DDH model[2]. Some of this discrepancy is no doubt due to nuclear physics uncertainties, but another source may be the use of the model-dependent DDH potential. A possible solution to these problems has recently been proposed by Zhu et al.[2, 3], restriction of experiments to nuclei with $A < 4$ so that nuclear uncertainties are minimal, and analysis using a model-independent picture via effective field theory. At low energies, less than $m_\pi^2/M_N \sim 20MeV$, such an approach is provided by Pionless EFT ($\text{EFT}_{\not\pi}$), which has been extremely successful at low energies in the two-body and three-body sector for parity-conserving (PC) interactions, including interactions with external currents[4]. At low energies inclusion of parity-violation requires only five additional low energy constants (LEC's) in the nucleon-nucleon interaction. These LEC's involve all possible isospin structures that mix S and P waves with one derivative and are equivalent to the parameters originally posited by Danilov[5]. The fact that five LEC's are needed has also been specifically shown by Girlanda, who does this by performing a non-relativistic reduction of all possible one derivative relativistic parity-violating (PV) structures that conserve CP[6]. Calculations for parity-violation using EFT methods have heretofore been primarily focused in the two-body sector. Such calculations include parity-violation in nucleon-nucleon scattering and in the radiative capture process $np \to d\gamma$[7–9]. PV EFT calculations have been done in the three-body sector using a hybrid approach, wherein the PV potential is given by $\text{EFT}_{\not\pi}$, but is used with wavefunctions determined by either a hypershperical harmonics method or by solving a differential Faddeev equation in configuration space[10, 11]. Such calculations include neutron spin rotation and beam asymmetry in $nd$ interactions. Recently a paper by Griesshammer, Schindler, and Springer predicted the spin rotation of a neutron on a deuterium target up to and including NLO effects in $\text{EFT}_{\not\pi}$[12]. However, they only included order of magnitude estimates for the PV coefficients and left open the calculation of other possible PV observables in $nd$ interactions. In this paper we set out to obtain estimates for the PV coefficients by matching them to the DDH "best" value estimates. As well as calculating the neutron spin rotation on a deuteron target at LO in $\text{EFT}_{\not\pi}$,

we also calculate the beam and target asymmetry at LO in $nd$ scattering. Estimation of these observables will then allow one to assess the feasibility of $nd$ interactions as a realistic experimental probe for the five PV LEC's. Below we calculate the LO amplitudes for S-P mixing in $nd$ scattering due to the two-body PV Lagrangian. (Since Griesshammer and Schindler showed that no three-body PV force occurs up to and including NLO, only five LEC's exist at LO[13].) Predictions are made for PV observables and numerical estimates are given based on DDH "best" value estimates. In a future publication we shall present higher order corrections. The paper is organized as follows. In section II we give the form of the two-body PV interaction. Then in section III we show what diagrams are needed at LO and how to calculate them. Section IV shows how estimates for PV LEC's can be obtained, and in Section V we show how to relate our amplitudes to observables. Finally in Section VI we summarize the results.

## II. Two-Body Parity-Violating Interaction

The leading order two-body PC Lagrangian in the auxiliary field formalism is given by

$$\begin{aligned}\mathcal{L}^d_{PC} = & N^\dagger \left( i\partial_0 + \frac{\vec{\nabla}^2}{2M_N} \right) N - t_i^\dagger \left( i\partial_0 + \frac{\vec{\nabla}^2}{4M_N} - \Delta^{(^3S_1)}_{(-1)} - \Delta^{(^3S_1)}_{(0)} \right) t_i + y_t \left[ t_i^\dagger N^T P_i N + h.c. \right] \\ & - s_a^\dagger \left( i\partial_0 + \frac{\vec{\nabla}^2}{4M_N} - \Delta^{(^1S_0)}_{(-1)} - \Delta^{(^1S_0)}_{(0)} \right) s_a + y_s \left[ s_a^\dagger N^T \bar{P}_a N + h.c. \right]\end{aligned} \tag{1}$$

where $t_i$ ($s_a$) is the deuteron (singlet) auxiliary field[14]. Here $P_i = \frac{1}{\sqrt{8}} \sigma_2 \sigma_i \tau_2$ projects out the $^3S_1$ channel and $\bar{P}_a = \frac{1}{\sqrt{8}} \sigma_2 \tau_2 \tau_a$ projects out the $^1S_0$ channel. The auxiliary field formalism is equivalent to the partial wave formalism in which only nucleon fields are used as can be seen by integrating over the auxiliary fields and using a field redefinition[15]. In this formulation the two-body PV Lagrangian amplitude is given by a form including five low energy constants[8].

FIG. 1: Infinite sum of nucleon bubbles contributes to LO deuteron propagator

$$
\begin{aligned}
\mathcal{L}^d_{PV} = -\Big[ & g^{(^3S_1-{}^1P_1)} t_i^\dagger \left( N^t \sigma_2 \tau_2 i \overset{\leftrightarrow}{\nabla}_i N \right) \\
& + g^{(^1S_0-{}^3P_0)}_{(\Delta I=0)} s_a^\dagger \left( N^T \sigma_2 \vec{\boldsymbol{\sigma}} \cdot \tau_2 \tau_a i \overset{\leftrightarrow}{\nabla} N \right) \\
& + g^{(^1S_0-{}^3P_0)}_{(\Delta I=1)} \epsilon^{3ab} (s^a)^\dagger \left( N^T \sigma_2 \vec{\boldsymbol{\sigma}} \cdot \tau_2 \tau^b \overset{\leftrightarrow}{\nabla} N \right) \\
& + g^{(^1S_0-{}^3P_0)}_{(\Delta I=2)} \mathcal{I}^{ab} (s^a)^\dagger \left( N^T \sigma_2 \vec{\boldsymbol{\sigma}} \cdot \tau_2 \tau^b i \overset{\leftrightarrow}{\nabla} N \right) \\
& + g^{(^3S_1-{}^3P_1)} \epsilon^{ijk} (t_i)^\dagger \left( N^T \sigma_2 \sigma^k \tau_2 \tau_3 \overset{\leftrightarrow^j}{\nabla} N \right) \Big] + h.c.
\end{aligned}
\tag{2}
$$

where $a \overset{\leftrightarrow}{\nabla} b = a(\overrightarrow{\nabla})b - (\overrightarrow{\nabla}a)b$, and $\mathcal{I} = \mathrm{diag}[1, 1, -2]$ projects out the isotensor contribution.

The deuteron kinetic energy and the term $\Delta^{(^3S_1)}_{(0)}$ are sub-leading with respect to $\Delta^{(^3S_1)}_{(-1)}$.(Letting $\Delta = \Delta^{(^3S_1)}_{(-1)} + \Delta^{(^3S_1)}_{(0)}$, the deuteron mass is given by $2M_N + \Delta$[16], and the term $\Delta$ is split up so as to not have to refit it at NLO.) Thus at LO the bare deuteron propagator is given by $i/\Delta^{(^3S_1)}_{(-1)}$ which is then dressed by an infinite number of nucleon bubbles as seen inf Fig. 1. The resulting propagator depends on $\Delta^{(^3S_1)}_{(-1)}$ and $y_t^2$, with values adjusted such that the deuteron propagator has its pole at the correct value. The values of $y_t^2$, $\Delta^{(^3S_1)}_{(-1)}$, $\Delta^{(^3S_1)}_{(0)}$ are then determined at NLO by making sure the deuteron pole position does not move and by reproducing the effective range expansion perturbatively at first order. A similar calculation can be carried out for the propagator of the singlet auxiliary field. This procedure has been carried out in many papers, the end results for the LO deuteron and singlet propagator are listed below[14]. Also we include the constraints imposed on the coefficients $y_t^2$, $\Delta^{(^3S_1)}_{(-1)}$, $\Delta^{(^3S_1)}_{(0)}$ and their $^1S_0$ counterparts at LO and NLO. Note the presence of the parameter $\mu$, which is a cutoff imposed by using dimensional regularization with the PDS subtraction scheme[17]. (Here $\gamma_t = 45.7025$ MeV is the deuteron binding momentum, $\gamma_s = 1/a_s$, where $a_s = -23.714$ fm is the scattering length in the $^1S_0$ channel, $\rho_t = 1.764$ fm is the effective range in the $^3S_1$ channel, and $r_{0s} = 2.73$ fm is the effective range in the $^1S_0$ channel.)

$$
iD_t(p_0, \vec{\mathbf{p}}) = \frac{4\pi i}{M_N y_t^2} \frac{1}{\gamma_t - \sqrt{\frac{\vec{\mathbf{p}}^2}{4} - M_N p_0 - i\epsilon}}
\tag{3}
$$

$$iD_s(p_0,\vec{\mathbf{p}}) = \frac{4\pi i}{M_N y_s^2}\frac{1}{\gamma_s - \sqrt{\frac{\vec{\mathbf{p}}^2}{4} - M_N p_0 - i\epsilon}} \tag{4}$$

$$\begin{aligned}
&\frac{\Delta^{(^3S_1)}_{(-1)}}{y_t^2} = \frac{M_N}{4\pi}(\gamma_t - \mu) && \frac{\Delta^{(^1S_0)}_{(-1)}}{y_s^2} = \frac{M_N}{4\pi}(\gamma_s - \mu) \\
&\Delta^{(^3S_1)}_{(0)} = \frac{\gamma_t^2}{M_N} && \Delta^{(^1S_0)}_{(0)} = 0 \\
&y_t^2 = \frac{8\pi}{M_N^2}\frac{1}{\rho_t} && y_s^2 = \frac{8\pi}{M_N^2}\frac{1}{r_{0s}}
\end{aligned} \tag{5}$$

## III. Three-Body Parity-Violation LO

As in the PC case for three-body interactions one needs to solve an infinite sum of diagrams for the PV amplitude at LO[14, 18], leading to a coupled set of integral equations. Numerical solution is necessary, as such integral equations cannot be solved analytically. In general we must solve a set of four coupled integral equations. However, since parity-violation is so small, $G_F m_\pi^2 \sim 10^{-7}$ we can ignore second order PV terms. Then the integral equations for the PC amplitudes decouple[19], and are exactly the same as in previous papers[14, 18, 20]. The remaining coupled PV integral equations at LO are shown in Fig. 2, where the boxes represent PV vertices, the double line the dressed deuteron propagator, the double dashed lines the dressed singlet propagator, and the line with arrow the nucleon propagator. The thick lines represent a sum over both deuteron and singlet propagators. Thus the thick line allows one to represent two Feynman diagrams with a single diagram. There are also diagrams where two dibaryon lines and two nucleon lines meet at a single vertex, due to the three-body force term in the Lagrangian.

This three-body force term enters at LO, only in the Doublet S-wave channel. (Note we have not yet projected out any specific channel.) The momentum integrals are regulated using a sharp cutoff $\Lambda$. The three-body force term is cutoff dependent. This cutoff is convenient because it can be implemented straightforwardly numerically. The three-body force term in the Doublet S wave channel is given by[21, 22]

$$\mathcal{H}(E,\Lambda) = \frac{2H_0(\Lambda)}{\Lambda^2} \tag{6}$$

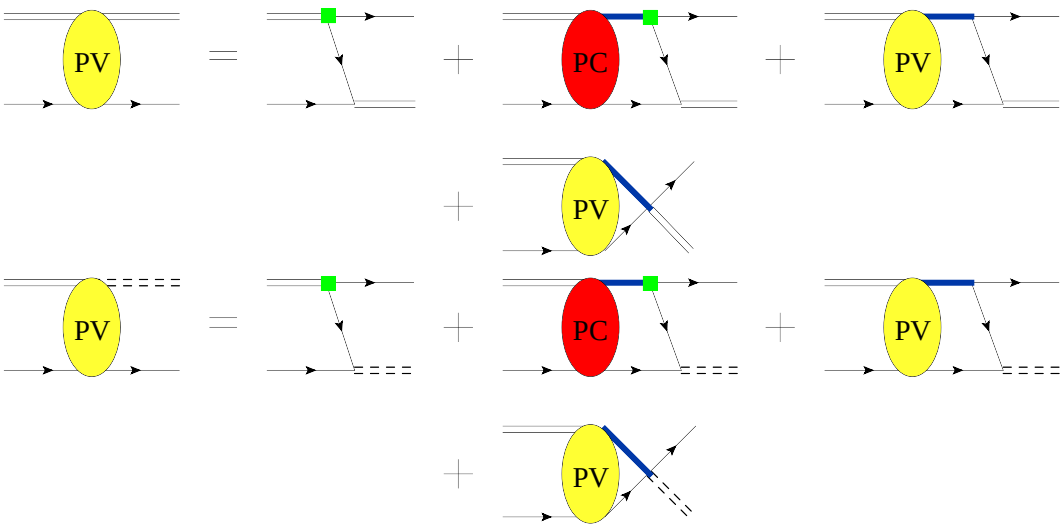


FIG. 2: (Color online)Integral Equations for Parity-Violation at LO (Note diagrams where lower vertices are PV are not included)

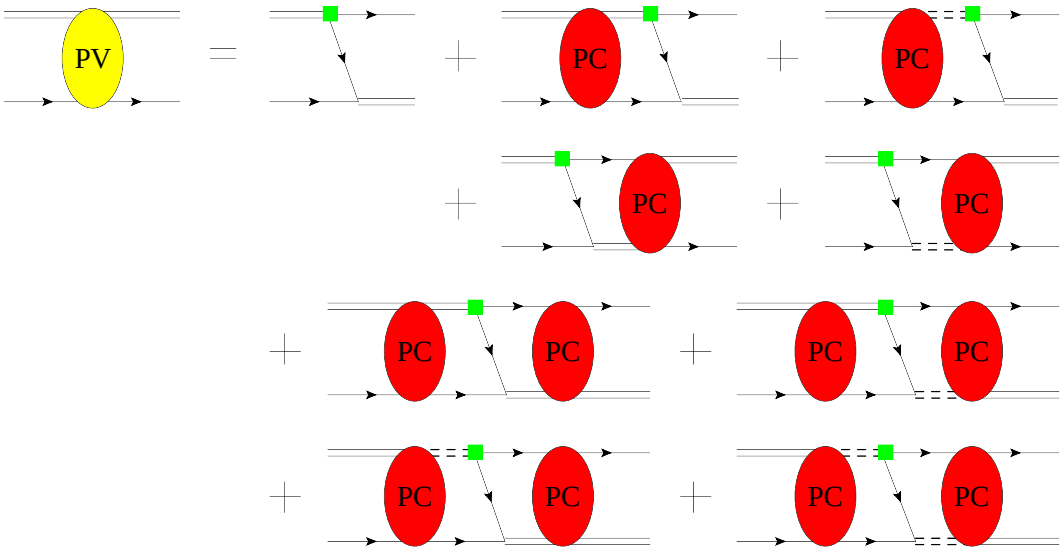


FIG. 3: (Color online) PV Diagrams at LO (Note diagrams where lower vertices are PV are not included)

The cutoff dependence of three-body force term $H_0(\Lambda)$ is chosen so that the Doublet S wave amplitude produces the correct scattering length[18, 20, 23]. (As noted earlier there is no need to include a PV three-body force, as it has been explicitly shown that no such term exists up to and including NLO[13].)

To first order in parity-violation the integral equation for the PV amplitude is given by the sum of diagrams shown in Fig. 3. The first diagram corresponds to a pure PV transition with no scattering in the initial or final channel. The next set of diagrams has a PV transition with scattering either in the initial or final channel but not both. (Also note that for these diagrams the singlet field acts as an intermediate state, which can only exist in the Doublet channel.) Finally we have the set of diagrams with a PV transition and scattering in both the final and initial channels.

Summing all of these figures one finds the PV amplitude given in Eq. (7), where $\vec{\mathbf{k}}$ is the incoming nucleon momentum and $\vec{\mathbf{p}}$ is the outgoing nucleon momentum in the c.m. frame. Since our diagrams are on shell we have $|\vec{\mathbf{k}}| = |\vec{\mathbf{p}}|$, and the total energy in the c.m. frame is given by $E = \frac{3\vec{\mathbf{k}}^2}{4M_N} - \frac{\gamma_t^2}{M_N}$. The vector index letter $w$ ($x$), represents the initial (final) deuteron auxiliary field polarization. Finally the Greek index $\alpha$ ($\beta$) is the initial (final) spinor index and $a$ ($b$) is the initial (final) isospinor index.

$$
\begin{aligned}
(it_{PV}^{xw})_{\alpha a}^{\beta b}(\vec{\mathbf{k}},\vec{\mathbf{p}}) = {} & \frac{4M_N}{\sqrt{8}}\frac{i}{\vec{\mathbf{k}}^2+\vec{\mathbf{k}}\cdot\vec{\mathbf{p}}+\vec{\mathbf{p}}^2-M_N E-i\epsilon}\left(\mathcal{K}_{PV}^{11\ xw}\right)_{\alpha a}^{\beta b}(\vec{\mathbf{p}},\vec{\mathbf{k}}) \qquad (7)\\
& + \frac{4M_N}{\sqrt{8}}\int\frac{d^4q}{(2\pi)^4}\mathbf{v}_p^T(i\tilde{\boldsymbol{\mathcal{K}}}^{xy})_{\gamma c}^{\beta b}(\vec{\mathbf{q}},\vec{\mathbf{p}},q_0)i\mathbf{D}\left(\frac{\vec{\mathbf{k}}^2}{4M_N}-\frac{\gamma_t^2}{M_N}+q_0,\vec{\mathbf{q}}\right)\left((it^{yw})_{\alpha a}^{\gamma c}(\vec{\mathbf{k}},\vec{\mathbf{q}})\right)\times\\
& \qquad \times\frac{i}{\frac{\vec{\mathbf{k}}^2}{2M_N}-q_0-\frac{\vec{\mathbf{q}}^2}{2M_N}+i\epsilon}\\
& + \frac{4M_N}{\sqrt{8}}\int\frac{d^4q}{(2\pi)^4}\left((it^{xy})_{\gamma c}^{\beta b}(\vec{\mathbf{p}},\vec{\mathbf{q}})\right)^T i\mathbf{D}\left(\frac{\vec{\mathbf{k}}^2}{4M_N}-\frac{\gamma_t^2}{M_N}+q_0,\vec{\mathbf{q}}\right)(i\tilde{\boldsymbol{\mathcal{K}}}^{yw})_{\alpha a}^{\gamma c}(\vec{\mathbf{k}},\vec{\mathbf{q}},q_0)\mathbf{v}_p\times\\
& \qquad \times\frac{i}{\frac{\vec{\mathbf{k}}^2}{2M_N}-q_0-\frac{\vec{\mathbf{q}}^2}{2M_N}+i\epsilon}\\
& + \frac{4M_N}{\sqrt{8}}\int\frac{d^4q}{(2\pi)^4}\int\frac{d^4\ell}{(2\pi)^4}\left((it^{xz})_{\delta d}^{\beta b}(\vec{\mathbf{p}},\vec{\boldsymbol{\ell}})\right)^T i\mathbf{D}\left(\frac{\vec{\mathbf{k}}^2}{4M_N}-\frac{\gamma_t^2}{M_N}+q_0,\vec{\mathbf{q}}\right)\\
& \qquad (i\tilde{\boldsymbol{\mathcal{K}}}^{zy})_{\gamma c}^{\delta d}(\vec{\mathbf{q}},\vec{\boldsymbol{\ell}},q_0+\ell_0)i\mathbf{D}\left(\frac{\vec{\mathbf{k}}^2}{4M_N}-\frac{\gamma_t^2}{M_N}+\ell_0,\vec{\boldsymbol{\ell}}\right)\left((it^{yw})_{\alpha a}^{\gamma c}(\vec{\mathbf{k}},\vec{\mathbf{q}})\right)\times\\
& \qquad \times\frac{i}{\frac{\vec{\mathbf{k}}^2}{2M_N}-q_0-\frac{\vec{\mathbf{q}}^2}{2M_N}+i\epsilon}\frac{i}{\frac{\vec{\mathbf{k}}^2}{2M_N}-\ell_0-\frac{\vec{\boldsymbol{\ell}}^2}{2M_N}+i\epsilon}
\end{aligned}
$$

The vector $\mathbf{v}_p$ projects out the nucleon-deuteron amplitude in cluster-configuration space and is defined as[20]

$$\mathbf{v}_p = \begin{pmatrix} 1 \\ 0 \end{pmatrix} \tag{8}$$

and the PC amplitudes $t$ are a vector defined as follows

$$\left( (it^{xw})^{\beta b}_{\alpha a} (\vec{\mathbf{k}}, \vec{\mathbf{q}}) \right) = \begin{pmatrix} (it^{xw}_{Nt\to Nt})^{\beta b}_{\alpha a} (\vec{\mathbf{k}}, \vec{\mathbf{q}}) \\ (it^{xw}_{Nt\to Ns})^{\beta b}_{\alpha a} (\vec{\mathbf{k}}, \vec{\mathbf{q}}) \end{pmatrix} \tag{9}$$

where $t_{Nt\to Nt}$ is the amplitude for $nd$ scattering and $t_{Nt\to Ns}$ is the amplitude for $nd$ going to a nucleon and a singlet combination of the remaining nucleons. (Note that we have not yet projected out Quartet or Doublet channels.) The expressions $\mathbf{D}(E, \vec{\mathbf{q}})$ and $(i\tilde{\boldsymbol{\mathcal{K}}}^{xw})^{\beta b}_{\alpha a}(\vec{\mathbf{q}}, \vec{\boldsymbol{\ell}}, q_0)$ are both matrices defined via.

$$i\mathbf{D}(E, \vec{\mathbf{q}}) = \begin{pmatrix} iD_t(E, \vec{\mathbf{q}}) & 0 \\ 0 & iD_s(E, \vec{\mathbf{q}}) \end{pmatrix} \tag{10}$$

$$\begin{aligned} (i\tilde{\boldsymbol{\mathcal{K}}}^{xw})^{\beta b}_{\alpha a}(\vec{\mathbf{q}}, \vec{\boldsymbol{\ell}}, q_0) =& \frac{i}{\frac{1}{2}\vec{\mathbf{q}}^2 + \vec{\mathbf{q}}\cdot\vec{\boldsymbol{\ell}} + \frac{1}{2}\vec{\boldsymbol{\ell}}^2 + \frac{1}{4}\vec{\mathbf{k}}^2 + \gamma_t^2 - M_N q_0 - i\epsilon} \times \\ & \times \begin{pmatrix} (\mathcal{K}^{11}_{PV}{}^{xw})^{\beta b}_{\alpha a} (\vec{\mathbf{q}}, \vec{\boldsymbol{\ell}}) & (\mathcal{K}^{12}_{PV}{}^{xw})^{\beta b}_{\alpha a} (\vec{\mathbf{q}}, \vec{\boldsymbol{\ell}}) \\ (\mathcal{K}^{21}_{PV}{}^{xw})^{\beta b}_{\alpha a} (\vec{\mathbf{q}}, \vec{\boldsymbol{\ell}}) & (\mathcal{K}^{22}_{PV}{}^{xw})^{\beta b}_{\alpha a} (\vec{\mathbf{q}}, \vec{\boldsymbol{\ell}}) \end{pmatrix} \end{aligned} \tag{11}$$

where the functions $\left(\mathcal{K}^{XY\,xw}_{PV}\right)^{\beta b}_{\alpha a} (\vec{\mathbf{q}}, \vec{\boldsymbol{\ell}})$, which contain all of the PV dependence are defined as

$$\begin{aligned} \left(\mathcal{K}^{11}_{PV}{}^{xw}\right)^{\beta b}_{\alpha a} (\vec{\mathbf{k}}, \vec{\mathbf{p}}) =& y_t g^{{}^3S_1 - {}^1P_1} (\sigma^x)^\beta_\alpha \delta^b_a (\vec{\mathbf{k}} + 2\vec{\mathbf{p}})^w + i y_d g^{{}^3S_1 - {}^3P_1} \epsilon^{w\ell y} (\sigma^y \sigma^x)^\beta_\alpha (\tau_3)^b_a (\vec{\mathbf{k}} + 2\vec{\mathbf{p}})^\ell \\ & + y_t g^{{}^3S_1 - {}^1P_1} (\sigma^w)^\beta_\alpha \delta^b_a (2\vec{\mathbf{k}} + \vec{\mathbf{p}})^x - i y_d g^{{}^3S_1 - {}^3P_1} \epsilon^{x\ell y} (\sigma^w \sigma^y)^\beta_\alpha (\tau_3)^b_a (2\vec{\mathbf{k}} + \vec{\mathbf{p}})^\ell \end{aligned} \tag{12a}$$

$$\begin{aligned} \left(\mathcal{K}^{12}_{PV}{}^{xA}\right)^{\beta b}_{\alpha a} (\vec{\mathbf{k}}, \vec{\mathbf{p}}) =& y_t g^{{}^1S_0 - {}^3P_0}_{(\Delta I=0)} (\sigma^\ell \sigma^x)^\beta_\alpha (\tau^A)^b_a (\vec{\mathbf{k}} + 2\vec{\mathbf{p}})^\ell + i y_d g^{{}^1S_0 - {}^3P_0}_{(\Delta I=1)} \epsilon^{3AC} (\sigma^\ell \sigma^x)^\beta_\alpha (\tau^C)^b_a (\vec{\mathbf{k}} + 2\vec{\mathbf{p}})^\ell \\ & + y_s g^{{}^3S_1 - {}^1P_1} \delta^\beta_\alpha (\tau^A)^b_a (2\vec{\mathbf{k}} + \vec{\mathbf{p}})^x - i y_t g^{{}^3S_1 - {}^3P_1} \epsilon^{x\ell y} (\tau^A \tau_3)^b_a (\sigma^y)^\beta_\alpha (2\vec{\mathbf{k}} + \vec{\mathbf{p}})^\ell \end{aligned} \tag{12b}$$

$$\begin{aligned} \left(\mathcal{K}^{21}_{PV}{}^{Bw}\right)^{\beta b}_{\alpha a} (\vec{\mathbf{k}}, \vec{\mathbf{p}}) =& y_s g^{{}^3S_1 - {}^1P_1} (\tau^B)^b_a \delta^\beta_\alpha (\vec{\mathbf{k}} + 2\vec{\mathbf{p}})^w + i y_t g^{{}^3S_1 - {}^3P_1} \epsilon^{w\ell y} (\sigma^y)^\beta_\alpha (\tau_3 \tau^B)^b_a (\vec{\mathbf{k}} + 2\vec{\mathbf{p}})^\ell \\ & + y_t g^{{}^1S_0 - {}^3P_0}_{(\Delta I=0)} (\sigma^w \sigma^\ell)^\beta_\alpha (\tau^B)^b_a (2\vec{\mathbf{k}} + \vec{\mathbf{p}})^\ell - i y_d g^{{}^1S_0 - {}^3P_0}_{(\Delta I=1)} \epsilon^{3BC} (\sigma^w \sigma^\ell)^\beta_b (\tau^C)^b_a (2\vec{\mathbf{k}} + \vec{\mathbf{p}})^\ell \end{aligned} \tag{12c}$$

$$\left(\mathcal{K}_{PV}^{22\ BA}\right)_{\alpha a}^{\beta b}(\vec{\mathbf{k}},\vec{\mathbf{p}}) = y_s g_{(\Delta I=0)}^{^1S_0-{}^3P_0}(\sigma^\ell)_\alpha^\beta(\tau^A\tau^B)_a^b(\vec{\mathbf{k}}+2\vec{\mathbf{p}})^\ell + iy_t g_{(\Delta I=1)}^{^1S_0-{}^3P_0}\epsilon^{3AC}(\sigma^\ell)_\alpha^\beta(\tau^C\tau^B)_a^b(\vec{\mathbf{k}}+2\vec{\mathbf{p}})^\ell \tag{12d}$$

$$+ y_s g_{(\Delta I=0)}^{^1S_0-{}^3P_0}(\tau^A\tau^B)_a^b(\sigma^\ell)_\alpha^\beta(2\vec{\mathbf{k}}+\vec{\mathbf{p}})^\ell - iy_t g_{(\Delta I=1)}^{^1S_0-{}^3P_0}\epsilon^{3BC}(\tau^A\tau^C)_a^b(\sigma^\ell)_\alpha^\beta(2\vec{\mathbf{k}}+\vec{\mathbf{p}})^\ell$$

(Note that the capital letters A, B, and C are used for the singlet auxiliary field polarization and the lowercase letters w, x, and y are used for the deuteron auxiliary field polarization.) Integrating over the energy and picking up the poles from the nucleon propagators in our diagrams Eq. (7) becomes.

$$\begin{aligned}
(t_{PV}^{xw})_{\alpha a}^{\beta b}(\vec{\mathbf{k}},\vec{\mathbf{p}}) = {} & \frac{4M_N}{\sqrt{8}}\mathbf{v}_p^T\,(\boldsymbol{\mathcal{K}}^{xw})_{\alpha a}^{\beta b}(\vec{\mathbf{k}},\vec{\mathbf{p}})\mathbf{v}_p \\
& - \frac{4M_N}{\sqrt{8}}\int\frac{d^3q}{(2\pi)^3}\mathbf{v}_p^T(\boldsymbol{\mathcal{K}}^{xy})_{\gamma c}^{\beta b}(\vec{\mathbf{q}},\vec{\mathbf{p}})\mathbf{D}\left(E-\frac{\vec{\mathbf{q}}^2}{2M_N},\vec{\mathbf{q}}\right)\left((t^{yw})_{\alpha a}^{\gamma c}(\vec{\mathbf{k}},\vec{\mathbf{q}})\right) \\
& - \frac{4M_N}{\sqrt{8}}\int\frac{d^3q}{(2\pi)^3}\left((t^{xy})_{\gamma c}^{\beta b}(\vec{\mathbf{q}},\vec{\mathbf{p}})\right)^T\mathbf{D}\left(E-\frac{\vec{\mathbf{q}}^2}{2M_N},\vec{\mathbf{q}}\right)(\boldsymbol{\mathcal{K}}^{yw})_{\alpha a}^{\gamma c}(\vec{\mathbf{k}},\vec{\mathbf{q}})\mathbf{v}_p \\
& + \frac{4M_N}{\sqrt{8}}\int\frac{d^3q}{(2\pi)^3}\int\frac{d^3\ell}{(2\pi)^3}\left((t^{xz})_{\delta d}^{\beta b}(\vec{\boldsymbol{\ell}},\vec{\mathbf{p}},)\right)^T\mathbf{D}\left(E-\frac{\vec{\mathbf{q}}^2}{2M_N},\vec{\mathbf{q}}\right) \\
& \qquad (\boldsymbol{\mathcal{K}}^{zy})_{\gamma c}^{\delta d}(\vec{\mathbf{q}},\vec{\boldsymbol{\ell}})\mathbf{D}\left(E-\frac{\vec{\boldsymbol{\ell}}^2}{2M_N},\vec{\boldsymbol{\ell}}\right)\left((t^{yw})_{\alpha a}^{\gamma c}(\vec{\mathbf{k}},\vec{\mathbf{q}})\right)
\end{aligned} \tag{13}$$

where

$$\begin{aligned}
(\boldsymbol{\mathcal{K}}^{xw})_{\alpha a}^{\beta b}(\vec{\mathbf{q}},\vec{\boldsymbol{\ell}}) = {} & \frac{1}{\vec{\mathbf{q}}^2+\vec{\mathbf{q}}\cdot\vec{\boldsymbol{\ell}}+\vec{\boldsymbol{\ell}}^2-M_NE-i\epsilon}\times \\
& \times\begin{pmatrix}(\mathcal{K}_{PV}^{11\ xw})_{\alpha a}^{\beta b}(\vec{\mathbf{q}},\vec{\boldsymbol{\ell}}) & (\mathcal{K}_{PV}^{12\ xw})_{\alpha a}^{\beta b}(\vec{\mathbf{q}},\vec{\boldsymbol{\ell}}) \\ (\mathcal{K}_{PV}^{21\ xw})_{\alpha a}^{\beta b}(\vec{\mathbf{q}},\vec{\boldsymbol{\ell}}) & (\mathcal{K}_{PV}^{22\ xw})_{\alpha a}^{\beta b}(\vec{\mathbf{q}},\vec{\boldsymbol{\ell}})\end{pmatrix}
\end{aligned} \tag{14}$$

Now that we have derived the PV amplitude, we note that it contains the related scattering amplitudes from the PC sector. Such PC scattering amplitudes are calculated in[20], by numerically solving Faddeev's equation in an angular momentum basis. However, as part of this solution one runs into singularities along the real axis. To overcome this difficulty the method of Hetherington and Schick is employed, in which the axis of integration is rotated into the complex plane, therefore avoiding the singularities[24–26]. One can then use the solutions along the deformed contour to solve for the amplitudes along the real axis. Details of the procedure to calculate these amplitudes can be found in[27]. In order to use the

solutions to Faddeev's equations we need to project out our PV amplitude into an angular momentum basis. However, unlike the PC sector, the PV amplitudes mix different angular momentum states. Also, since at leading order, spin and orbital angular momentum mix, the appropriate angular momentum basis to use is the total angular momentum $\vec{\mathbf{J}} = \vec{\mathbf{L}} + \vec{\mathbf{S}}$. Thus we express our PV amplitude as

$$t_{PV}(\vec{\mathbf{k}}, \vec{\mathbf{p}}) = \sum_{J=0}^{\infty} \sum_{M=-J}^{M=J} \sum_{L=|J-S|}^{J+S} \sum_{L'=|J-S'|}^{J+S'} \sum_{S,S'} 4\pi t^{JM}_{L'S',LS}(k,p) \mathscr{Y}^{M}_{J,L'S'}(\hat{\mathbf{p}}) \left(\mathscr{Y}^{M}_{J,LS}(\hat{\mathbf{k}})\right)^* \tag{15}$$

where the spin angle functions are given by

$$\mathscr{Y}^{M}_{J,LS}(\hat{\mathbf{k}}) = \sum_{m_L, m_S} C^{JM}_{Lm_L,Sm_S} Y^{m_L}_{L}(\hat{\mathbf{k}}) \chi^{m_S}_{S} \tag{16}$$

$\chi^{m_S}_S$ being the spinor part of the spin-angle functions, $C^{JM}_{Lm_L,Sm_S}$ the appropriate Clebsch-Gordan coefficient, and $Y^{m_L}_L(\hat{\mathbf{k}})$ the appropriate spherical harmonic. Since the spin-angle functions are orthogonal, we can project out the amplitudes in our angular momentum basis via

$$t^{JM}_{L'S',LS}(k,p) = \frac{1}{4\pi} \int d\Omega_k \int d\Omega_p \left(\mathscr{Y}^{M}_{J,L'S'}(\hat{\mathbf{p}})\right)^* t_{PV}(\vec{\mathbf{k}}, \vec{\mathbf{p}}) \mathscr{Y}^{M}_{J,LS}(\hat{\mathbf{k}}) \tag{17}$$

At sufficiently low energies S-P mixing will dominate. Thus we will calculate only the amplitudes $t^{SM}_{1S',0S}$ (Note J=S here since L=0) for all possible values of $S$ and $S'$. All spin and angle dependence is contained within the matrix $(\boldsymbol{\mathcal{K}}^{xw})^{\beta b}_{\alpha a}(\vec{\mathbf{q}}, \vec{\boldsymbol{\ell}})$, and the appropriate projections in $\vec{\mathbf{J}}$, $\vec{\mathbf{L}}$,and $\vec{\mathbf{S}}$ can be found in the appendix. Going to a partial wave basis we finally obtain an expression for the PV partial wave amplitudes.

$$\begin{aligned}
t_{PV}{}^{JM}_{L'S',LS}(k,p) = {} & \frac{M_N}{\sqrt{8}\pi} \mathbf{v}_p^T \boldsymbol{\mathcal{K}}(k,p)^J_{L'S',LS} \mathbf{v}_p + \\
& - \frac{M_N}{2\sqrt{8}\pi^3} \int_0^\infty dq q^2 \mathbf{v}_p^T \boldsymbol{\mathcal{K}}(q,p)^J_{L'S',LS} \mathbf{D}\left(E - \frac{\vec{\mathbf{q}}^2}{2M_N}, \vec{\mathbf{q}}\right) \left(t_{PC}{}^{JM}_{LS,LS}(k,q)\right) \\
& - \frac{M_N}{2\sqrt{8}\pi^3} \int_0^\infty dq q^2 \left(t_{PC}{}^{JM}_{L'S',L'S'}(q,p)\right)^T \mathbf{D}\left(E - \frac{\vec{\mathbf{q}}^2}{2M_N}, \vec{\mathbf{q}}\right) \boldsymbol{\mathcal{K}}(k,q)^J_{L'S',LS} \mathbf{v}_p \\
& + \frac{M_N}{4\sqrt{8}\pi^5} \int_0^\infty dq q^2 \int_0^\infty d\ell \ell^2 \left(t_{PC}{}^{JM}_{L'S',L'S'}(p,\ell)\right)^T \mathbf{D}\left(E - \frac{\vec{\mathbf{q}}^2}{2M_N}, \vec{\mathbf{q}}\right) \\
& \quad \boldsymbol{\mathcal{K}}(q,\ell)^{JM}_{L'S',LS} \mathbf{D}\left(E - \frac{\vec{\boldsymbol{\ell}}^{\mathbf{2}}}{2M_N}, \vec{\boldsymbol{\ell}}\right) \left(t_{PC}{}^{JM}_{LS,LS}(k,q)\right)
\end{aligned} \tag{18}$$

This expression contains the PC amplitudes in the partial wave basis of total angular momentum $\vec{\mathbf{J}} = \vec{\mathbf{L}} + \vec{\mathbf{S}}$. (These are equivalent to the PC amplitudes in the partial wave basis of orbital angular momentum.) It can be shown straightforwardly that the PC amplitudes are independent of total angular momentum $\vec{\mathbf{J}}$. Thus we can use the PC amplitudes as calculated numerically by[14, 18, 20] and perform the integration numerically in order to obtain the associated PV amplitudes.

Before integrating Eq. (18) we multiply by the LO deuteron renormalization $Z_D = (8\pi\gamma_d)/(M_N^2 y_t^2)$[14], and use the renormalized PC amplitudes. We find that all the PV LEC's occur in the combinations.

$$\frac{g^{^3S_1-{}^1P_1}}{y_t}, \frac{g^{^3S_1-{}^3P_1}}{y_t}, \frac{g^{^1S_0-{}^3P_0}_{(\Delta I=0)}}{y_s}, \frac{g^{^1S_0-{}^3P_0}_{(\Delta I=1)}}{y_s}$$

(Note $g^{^1S_0-{}^3P_0}_{(\Delta I=2)}$ does not appear as a $\Delta I = 2$ transition is not allowed for a first order PV transition in $nd$ scattering.) For the sake of convenience we find it useful to make the following definitions.

$$g_1 = \frac{g^{^3S_1-{}^1P_1}}{y_t}, g_2 = \frac{g^{^3S_1-{}^3P_1}}{y_t}, g_3 = \frac{g^{^1S_0-{}^3P_0}_{(\Delta I=0)}}{y_s}, g_4 = \frac{g^{^1S_0-{}^3P_0}_{(\Delta I=1)}}{y_s}, g_5 = \frac{g^{^1S_0-{}^3P_0}_{(\Delta I=2)}}{y_s}$$

Since these coefficients are unknown, we will write the PV partial wave amplitudes as follows, where $\left(t_{PV}{}^{JM}_{L'S',LS}(k,p)\right)^i$ is calculated by setting $g_j = 0, j \neq i$ and $g_i = 1$ in the PV partial wave amplitude. Thus the PV amplitude can be written as.

$$t_{PV}{}^{JM}_{L'S',LS}(k,p) = \sum_{i=1}^{4} g_i \left(t_{PV}{}^{JM}_{L'S',LS}(k,p)\right)^i \tag{19}$$

## IV. Parity-Violating Potential

It is clear from Eq. (19) that in order to obtain numerical values for the PV amplitude one needs to know the size of the coefficients $g_i$, which at this time are not determined from either theory or experiment. Nevertheless, we can obtain estimates by matching the $g_i$ onto the familiar DDH coefficients. We will carry out this procedure in three steps. First we match the DDH coefficients onto the coefficients of the Zhu potential[3]. Then we match the Zhu potential on to the Girlanda potential[10]. Finally we project the coefficients of the Girlanda potential onto the coefficients of the auxiliary field formalism. We also show how all these formalisms can be matched to the familiar Danilov parameters

The DDH model[1] is a single-meson-exchange picture, limited to exchange of the lightest mesons $\pi$, $\rho$, and $\omega$.[1] The strong Hamiltonian is given by

$$\begin{aligned}\mathcal{H}_{st} =& ig_{\pi NN}\bar{N}\gamma_5\tau\cdot\pi N + g_\rho\bar{N}\left(\gamma_\mu + i\frac{(1+\chi_\rho)}{2M_N}\sigma_{\mu\nu}k^\nu\right)\tau\cdot\rho^\mu N \\ &+ g_\omega\bar{N}\left(\gamma_\mu + i\frac{(1+\chi_\omega)}{2M_N}\sigma_{\mu\nu}k^\nu\right)\omega^\mu N\end{aligned} \tag{20}$$

with the strong couplings given approximately by $g^2_{\pi NN}/4\pi \simeq 13.5$ and $g^2_\rho/4\pi = \frac{1}{9}g^2_\omega/4\pi \simeq .67$, while the magnetic moment terms are approximately $\chi_\rho = \kappa_p - \kappa_n = 3.7$ and $\chi_\omega = \kappa_p + \kappa_n = -.12$. The phenomenological weak interaction Hamiltonian posited by DDH consists of seven weak coupling terms

$$\begin{aligned}\mathcal{H}_{wk} =& i\frac{f^1_\pi}{\sqrt{2}}\bar{N}(\tau\times\pi)_z N + \bar{N}\left(h^0_\rho\tau\cdot\rho^\mu + h^1_\rho\rho^\mu_z + \frac{g^2_\rho}{2\sqrt{6}}(3\tau_z\rho^\mu_z - \tau\cdot\rho^\mu)\right)\gamma_\mu\gamma_5 N \\ &+ \bar{N}\left(h^0_\omega\omega^\mu + h^1_\omega\tau_z\omega^\mu\right)\gamma_\mu\gamma_5 N - h'^1_\rho\bar{N}(\tau\times\rho^\mu)_z\frac{\sigma_{\mu\nu}k^\nu}{2M_N}\gamma_5 N\end{aligned} \tag{21}$$

DDH attempted to obtain theoretical predictions for the seven constants using SU(6) symmetry and quark model techniques. However, due to the difficulty of this calculation they were only able to come up with reasonable ranges and "best" values as shown in Table I. (Also shown are estimates by other groups.)

| | DDH[1] | DDH[1] | DZ[29] | FCDH[30] |
|---|---|---|---|---|
| Coupling | Reasonable Range | "Best" Value | | |
| $f_\pi$ | $0 \to 30$ | +12 | +3 | +7 |
| $h^0_\rho$ | $30 \to -81$ | -30 | -22 | -10 |
| $h^1_\rho$ | $-1 \to 0$ | -.5 | +1 | -1 |
| $h^2_\rho$ | $-20 \to -29$ | -25 | -18 | -18 |
| $h^0_\omega$ | $15 \to -27$ | -5 | -10 | -13 |
| $h^1_\omega$ | $-5 \to -2$ | -3 | -6 | -6 |

TABLE I: Weak NNM couplings. All numbers are quoted in units of the "sum rule" value $S_R = 3.8 \times 10^{-8}$

[1] Since CP is conserved there are no neutral pseudoscalar mesons $\pi^0$, $\eta$, or $\eta'$ by Barton's theorem[28]

The form of any PV potential can be written as a sum of operators $O_{ij}^{(n)}$ with corresponding coefficients $c_n^\alpha$, where $\alpha$ refers to the specific potential of interest..

$$V_{ij}^\alpha = \sum_n c_n^\alpha O_{ij}^{(n)} \tag{22}$$

At the lowest energies the component of the operators that contain momentum is of two forms.

$$\begin{aligned} \mathbf{X}_{ij,+}^{(n)} &= \{\vec{\mathbf{p}}_{ij}, f_n^\alpha(r_{ij})\} \\ \mathbf{X}_{ij,-}^{(n)} &= i[\vec{\mathbf{p}}_{ij}, f_n^\alpha(r_{ij})] \end{aligned} \tag{23}$$

where $\vec{\mathbf{p}}_{ij} = (\vec{\mathbf{p}}_1 - \vec{\mathbf{p}}_2)/2$ is the momentum of the nucleon-nucleon system in the c.m. frame. The coefficients, operators, and regulator functions $f_n^{DDH}(r_{ij})$ for the DDH potential and $f_n^{Zhu}(r_{ij})$ for the Zhu potential are given in Table II. The functions $f_n^{DDH}(r_{ij})$ are Yukawa functions, where the mass corresponds to the appropriate meson[2]. However, at the lowest energies the functions for the DDH potential can be written as $f_i(r) = \frac{1}{m_i^2}\delta^3(\vec{\mathbf{r}})$, where $i = \pi$,$\rho$, or $\omega$[2]. Likewise the functions $f_m(r) = \frac{1}{m^2}\delta^3(\vec{\mathbf{r}})$ for the Zhu potential become delta functions in the low energy limit, where $m$ is a mass sufficiently greater than our energies of interest such that the delta function approximation is valid (for our low energies of interest $m = m_\pi$ is sufficient). Thus at low energies the DDH potential and the Zhu potential can be trivially matched yielding[3]

$$\frac{\tilde{C}_1}{C_1} = \frac{\tilde{C}_2}{C_2} = 1 + \chi_\omega \simeq .88 \tag{24}$$

$$\frac{\tilde{C}_3}{C_3} = \frac{\tilde{C}_4}{C_4} = \frac{\tilde{C}_5}{C_5} = 1 + \chi_\rho \simeq 4.7 \tag{25}$$

TABLE II: PV potential in DDH and Zhu formalism. $\mathcal{T}_{ij} \equiv (3\tau_i^z\tau_j^z - \tau_i\cdot\tau_j)$. (Note $\Lambda_\chi \sim 4\pi F_\pi$ is the chiral scale[31, 32], where $F_\pi = 92.4MeV$ is the pion decay constant)

| $n$ | $c_n^{DDH}$ | $c_n^{Zhu}$ | $f_n^{DDH}(r)$ | $f_n^{Zhu}$ | $O_{ij}^{(n)}$ |
|---|---|---|---|---|---|
| 1 | $+\frac{g_{\pi NN}}{2\sqrt{2}M_N}f_\pi$ | $\frac{m^2}{\Lambda_\chi^3}2\tilde{C}_6$ | $f_\pi(r)$ | $f_m(r)$ | $(\tau_i\times\tau_j)^z(\vec{\boldsymbol{\sigma}}_i+\vec{\boldsymbol{\sigma}}_j)\cdot\boldsymbol{X}_{ij,-}^{(1)}$ |
| 2 | $-\frac{g_\rho}{M_N}h_\rho^0$ | $\frac{m^2}{\Lambda_\chi^3}2C_3$ | $f_\rho(r)$ | $f_m(r)$ | $(\tau_i\cdot\tau_j)(\vec{\boldsymbol{\sigma}}_i-\vec{\boldsymbol{\sigma}}_j)\cdot\boldsymbol{X}_{ij,+}^{(2)}$ |
| 3 | $-\frac{g_\rho(1+\chi_\rho)}{M_N}h_\rho^0$ | $\frac{m^2}{\Lambda_\chi^3}2\tilde{C}_3$ | $f_\rho(r)$ | $f_m(r)$ | $(\tau_i\cdot\tau_j)(\vec{\boldsymbol{\sigma}}_i\times\vec{\boldsymbol{\sigma}}_j)\cdot\boldsymbol{X}_{ij,-}^{(3)}$ |
| 4 | $-\frac{g_\rho}{2M_N}h_\rho^1$ | $\frac{m^2}{\Lambda_\chi^3}C_4$ | $f_\rho(r)$ | $f_m(r)$ | $(\tau_i+\tau_j)^z(\vec{\boldsymbol{\sigma}}_i-\vec{\boldsymbol{\sigma}}_j)\cdot\boldsymbol{X}_{ij,+}^{(4)}$ |
| 5 | $-\frac{g_\rho(1+\chi_\rho)}{2M_N}h_\rho^1$ | $\frac{m^2}{\Lambda_\chi^3}\tilde{C}_4$ | $f_\rho(r)$ | $f_m(r)$ | $(\tau_i+\tau_j)^z(\vec{\boldsymbol{\sigma}}_i\times\vec{\boldsymbol{\sigma}}_j)\cdot\boldsymbol{X}_{ij,-}^{(5)}$ |
| 6 | $-\frac{g_\rho}{2\sqrt{6}M_N}h_\rho^2$ | $-\frac{m^2}{\Lambda_\chi^3}2C_5$ | $f_\rho(r)$ | $f_m(r)$ | $\mathcal{T}_{ij}(\vec{\boldsymbol{\sigma}}_i-\vec{\boldsymbol{\sigma}}_j)\cdot\boldsymbol{X}_{ij,+}^{(6)}$ |
| 7 | $-\frac{g_\rho(1+\chi_\rho)}{2\sqrt{6}M_N}h_\rho^2$ | $-\frac{m^2}{\Lambda_\chi^3}2\tilde{C}_5$ | $f_\rho(r)$ | $f_m(r)$ | $\mathcal{T}_{ij}(\vec{\boldsymbol{\sigma}}_i\times\vec{\boldsymbol{\sigma}}_j)\cdot\boldsymbol{X}_{ij,-}^{(7)}$ |
| 8 | $-\frac{g_\omega}{M_N}h_\omega^0$ | $\frac{m^2}{\Lambda_\chi^3}2C_1$ | $f_\omega(r)$ | $f_m(r)$ | $(\vec{\boldsymbol{\sigma}}_i-\vec{\boldsymbol{\sigma}}_j)\cdot\boldsymbol{X}_{ij,+}^{(8)}$ |
| 9 | $-\frac{g_\omega(1+\chi_\omega)}{M_N}h_\omega^0$ | $\frac{m^2}{\Lambda_\chi^3}2\tilde{C}_1$ | $f_\omega(r)$ | $f_m(r)$ | $(\vec{\boldsymbol{\sigma}}_i\times\vec{\boldsymbol{\sigma}}_j)\cdot\boldsymbol{X}_{ij,-}^{(9)}$ |
| 10 | $-\frac{g_\omega}{2M_N}h_\omega^1$ | $\frac{m^2}{\Lambda_\chi^3}C_2$ | $f_\omega(r)$ | $f_m(r)$ | $(\tau_i+\tau_j)^z(\vec{\boldsymbol{\sigma}}_i-\vec{\boldsymbol{\sigma}}_j)\cdot\boldsymbol{X}_{ij,+}^{(10)}$ |
| 11 | $-\frac{g_\omega(1+\chi_\omega)}{2M_N}h_\omega^1$ | $\frac{m^2}{\Lambda_\chi^3}\tilde{C}_2$ | $f_\omega(r)$ | $f_m(r)$ | $(\tau_i+\tau_j)^z(\vec{\boldsymbol{\sigma}}_i\times\vec{\boldsymbol{\sigma}}_j)\cdot\boldsymbol{X}_{ij,-}^{(11)}$ |
| 12 | $-\frac{g_\omega h_\omega^1 - g_\rho h_\rho^1}{2M_N}$ | $\frac{m^2}{\Lambda_\chi^3}(C_2-C_4)$ | $f_\rho(r)$ | $f_m(r)$ | $(\tau_i-\tau_j)^z(\vec{\boldsymbol{\sigma}}_i+\vec{\boldsymbol{\sigma}}_j)\cdot\boldsymbol{X}_{ij,+}^{(12)}$ |
| 13 | $-\frac{g_\rho}{2M_N}h_\rho'^1$ | 0 | $f_\rho(r)$ | 0 | $(\tau_i\times\tau_j)^z(\vec{\boldsymbol{\sigma}}_i+\vec{\boldsymbol{\sigma}}_j)\cdot\boldsymbol{X}_{ij,-}^{(13)}$ |

$$
\begin{aligned}
C_1^{DDH} &= -\frac{\Lambda_\chi^3}{2M_N m_\omega^2} g_\omega h_\omega^0 \overset{\text{bestguess}}{\longrightarrow} 2.25\times 10^{-6} \\
C_2^{DDH} &= -\frac{\Lambda_\chi^3}{2M_N m_\omega^2} g_\omega h_\omega^1 \overset{\text{bestguess}}{\longrightarrow} 1.35\times 10^{-6} \\
C_3^{DDH} &= -\frac{\Lambda_\chi^3}{2M_N m_\rho^2} g_\rho h_\rho^0 \overset{\text{bestguess}}{\longrightarrow} 4.58\times 10^{-6} \\
C_4^{DDH} &= -\frac{\Lambda_\chi^3}{2M_N m_\rho^2} g_\rho h_\rho^1 \overset{\text{bestguess}}{\longrightarrow} 7.64\times 10^{-8} \\
C_5^{DDH} &= \frac{\Lambda_\chi^3}{4\sqrt{6}M_N m_\rho^2} g_\rho h_\rho^0 \overset{\text{bestguess}}{\longrightarrow} -7.80\times 10^{-7} \\
\tilde{C}_6^{DDH} &\simeq \frac{\Lambda_\chi^3}{4\sqrt{2}M_N m_\pi^2} g_{\pi NN} f_\pi \overset{\text{bestguess}}{\longrightarrow} 9.19\times 10^{-5}
\end{aligned}
\tag{26}
$$

As first pointed out by Danilov, one needs five PV terms at the lowest energies in the two-body sector[5], since only S-P mixing is involved. By conservation of angular momentum the state ${}^3S_1$, can only connect with the states ${}^1P_1$ or ${}^3P_1$. Since ${}^3S_1$ is an isosinglet there is a unique way to get to the isosinglet state ${}^1P_1$ and isotriplet state ${}^3P_1$. Similarly, the state ${}^1S_0$ can only connect with the state ${}^3P_0$. However, both ${}^1S_0$ and ${}^3P_0$ are isotriplet states so the operator connecting these states can carry $\Delta I = 0, 1$, or 2. The existence of five unique operators which characterize parity-violation at low energy appears to be in contradiction with the DDH and Zhu potential, which involve ten different operators. However, at low energies five of these operator structures are redundant as shown by Girlanda[6]. In this procedure one begins with all possible one-derivative P violating CP conserving relativistic terms.

$$
\begin{aligned}
\mathcal{O}_1 &= \bar{\psi}\gamma^\mu\psi\bar{\psi}\gamma_\mu\gamma_5\psi & \tilde{\mathcal{O}}_1 &= \bar{\psi}\gamma^\mu\gamma_5\psi\partial^\nu(\bar{\psi}\sigma_{\mu\nu}\psi) \\
\mathcal{O}_2 &= \bar{\psi}\gamma^\mu\psi\bar{\psi}\tau_3\gamma_\mu\gamma_5\psi & \tilde{\mathcal{O}}_2 &= \bar{\psi}\gamma^\mu\gamma_5\psi\partial^\nu(\bar{\psi}\tau_3\sigma_{\mu\nu}\psi) \\
\mathcal{O}_3 &= \bar{\psi}\tau_a\gamma^\mu\psi\bar{\psi}\tau^a\gamma_\mu\gamma_5\psi & \tilde{\mathcal{O}}_3 &= \bar{\psi}\tau_a\gamma^\mu\gamma_5\psi\partial^\nu(\bar{\psi}\tau^a\sigma_{\mu\nu}\psi) \\
\mathcal{O}_4 &= \bar{\psi}\tau_3\gamma^\mu\psi\bar{\psi}\gamma_\mu\gamma_5\psi & \tilde{\mathcal{O}}_4 &= \bar{\psi}\tau_3\gamma^\mu\gamma_5\psi\partial^\nu(\bar{\psi}\sigma_{\mu\nu}\psi) \\
\mathcal{O}_5 &= \mathcal{I}_{ab}\bar{\psi}\tau_a\gamma^\mu\psi\bar{\psi}\tau_b\gamma_\mu\gamma_5\psi & \tilde{\mathcal{O}}_5 &= \mathcal{I}_{ab}\bar{\psi}\tau_a\gamma^\mu\gamma_5\psi\partial^\nu(\bar{\psi}\tau_b\sigma_{\mu\nu}\psi) \\
\mathcal{O}_6 &= i\epsilon_{ab3}\bar{\psi}\tau_a\gamma^\mu\psi\bar{\psi}\tau_b\gamma_\mu\gamma_5\psi & \tilde{\mathcal{O}}_6 &= i\epsilon_{ab3}\bar{\psi}\tau_a\gamma^\mu\gamma_5\psi\partial^\nu(\bar{\psi}\tau_b\sigma_{\mu\nu}\psi)
\end{aligned}
\tag{27}
$$

Using Fierz transformations and the equations of motion, there exist six identities

$$\begin{aligned} \mathcal{O}_3 =& \mathcal{O}_1 & \tilde{\mathcal{O}}_2 + \tilde{\mathcal{O}}_4 =& M_N(\mathcal{O}_2 + \mathcal{O}_4) \\ \mathcal{O}_2 - \mathcal{O}_4 =& 2\mathcal{O}_6 & \tilde{\mathcal{O}}_2 - \tilde{\mathcal{O}}_4 =& -2M_N\mathcal{O}_6 - \tilde{\mathcal{O}}_6 \\ \tilde{\mathcal{O}}_3 + 3\tilde{\mathcal{O}}_1 =& 2M_N(\mathcal{O}_1 + \mathcal{O}_3) & \tilde{\mathcal{O}}_5 =& M_N\mathcal{O}_5 \end{aligned} \tag{28}$$

reducing the number of unique operators to six. However, in a non-relativistic reduction it turns out that two of the operators have equivalent structures leaving five unique operators at the lowest energies. The resulting PV Lagrangian in the Girlanda formalism is given by

$$\begin{aligned} \mathcal{L}_{\rm PV}^{\rm Gir} =& \mathcal{G}_1(N^\dagger\vec{\boldsymbol{\sigma}}N\cdot N^\dagger i\overset{\leftrightarrow}{\nabla}N - N^\dagger NN^\dagger i\overset{\leftrightarrow}{\nabla}\cdot\vec{\boldsymbol{\sigma}}N) - \tilde{\mathcal{G}}_1\epsilon_{ijk}N^\dagger\sigma_i N\nabla_j(N^\dagger\sigma_k N) \\ &- \mathcal{G}_2\epsilon_{ijk}[N^\dagger\tau_3\sigma_i N\nabla_j(N^\dagger\sigma_k N) + N^\dagger\sigma_i N\nabla_j(N^\dagger\tau_3\sigma_k N)] \\ &- \tilde{\mathcal{G}}_5\mathcal{I}_{ab}\epsilon_{ijk}N^\dagger\tau_a\sigma_i N\nabla_j(N^\dagger\tau_b\sigma_k N) + \mathcal{G}_6\epsilon_{ab3}\overset{\rightarrow}{\nabla}(N^\dagger\tau_a N)\cdot N^\dagger\tau_b\vec{\boldsymbol{\sigma}}N \end{aligned} \tag{29}$$

(In Eq. (29) a factor of $1/\Lambda_\chi^3$ has been absorbed into the coefficients. This notation agrees with the notation of Phillips, Schindler, and Springer[7].) With this PV Lagrangian one can compute the Girlanda potential which takes on the following form given by Eq. (22), where $n$ runs from one to five, and $\mu$ is a mass chosen to be much larger than the energies of interest (again for our purposes we choose $\mu = m_\pi$).

TABLE III: PV potential in Girlanda formalism. $\mathcal{T}_{ij} \equiv (3\tau_i^z\tau_j^z - \tau_i\cdot\tau_j)$.

| $n$ | $c_n^{Gir}$ | $f_n^{Gir}(r)$ | $O_{ij}^{(n)}$ |
|---|---|---|---|
| 1 | $-\mu^2\mathcal{G}_6$ | $\frac{1}{\mu^2}\delta^3(\vec{\mathbf{r}})$ | $(\tau_i\times\tau_j)^z(\vec{\boldsymbol{\sigma}}_i + \vec{\boldsymbol{\sigma}}_j)\cdot\boldsymbol{X}_{ij,-}^{(1)}$ |
| 2 | $2\mu^2\mathcal{G}_2$ | $\frac{1}{\mu^2}\delta^3(\vec{\mathbf{r}})$ | $(\tau_i+\tau_j)^z(\vec{\boldsymbol{\sigma}}_i - \vec{\boldsymbol{\sigma}}_j)\cdot\boldsymbol{X}_{ij,+}^{(2)}$ |
| 3 | $-2\mu^2\mathcal{G}_5$ | $\frac{1}{\mu^2}\delta^3(\vec{\mathbf{r}})$ | $\mathcal{T}_{ij}(\vec{\boldsymbol{\sigma}}_i - \vec{\boldsymbol{\sigma}}_j)\cdot\boldsymbol{X}_{ij,+}^{(3)}$ |
| 4 | $2\mu^2\mathcal{G}_1$ | $\frac{1}{\mu^2}\delta^3(\vec{\mathbf{r}})$ | $(\vec{\boldsymbol{\sigma}}_i - \vec{\boldsymbol{\sigma}}_j)\cdot\boldsymbol{X}_{ij,+}^{(4)}$ |
| 5 | $2\mu^2\tilde{\mathcal{G}}_1$ | $\frac{1}{\mu^2}\delta^3(\vec{\mathbf{r}})$ | $(\vec{\boldsymbol{\sigma}}_i\times\vec{\boldsymbol{\sigma}}_j)\cdot\boldsymbol{X}_{ij,-}^{(5)}$ |

Using (28) one can reduce the Zhu potential to a set of five operators, allowing the matching of the Zhu coefficients onto the Girlanda coefficients as shown in Table V.

For our calculations, we also require the coefficients in the auxiliary field formalism Eq. (2). This matching of the $\mathcal{G}_i$ and $g_i$ requires two steps. One first performs Gaussian integration over the auxiliary fields followed by a field redefinition to rewrite the Lagrangian, Eq (2) in terms of nucleon fields, as done by Schindler, and Springer[8]. Then one can match this partial wave formalism onto the Girlanda formalism by performing Fierz rearrangements and using the constraints Eq. (28) with a non-relativistic reduction, yielding the results in Table V (This has also been done using a different method by Phillips, Schindler, and Springer[7].)

Finally we wish to match the Girlanda potential onto the Danilov potential which is given by Eq. (22) in Table IV, where $n$ runs from one to five.

TABLE IV: PV potential in Danilov formalism. $\mathcal{T}_{ij} \equiv (3\tau_i^z\tau_j^z - \tau_i \cdot \tau_j)$, $P_0 = \frac{1}{4}(1 - \vec{\boldsymbol{\sigma}}_i \cdot \vec{\boldsymbol{\sigma}}_j)$, $P_1 = \frac{1}{4}(3 + \vec{\boldsymbol{\sigma}}_i \cdot \vec{\boldsymbol{\sigma}}_j)$, and $a_t = 5.314$ fm is the ${}^3S_1$ scattering length.

| $n$ | $c_n^{Dan}$ | $f_n^{Dan}(r)$ | $O_{ij}^{(n)}$ |
|---|---|---|---|
| 1 | $\frac{1}{2}a_t\rho_t$ | $\frac{4\pi}{M_N}\delta^3(\vec{\mathbf{r}})$ | $(\tau_i - \tau_j)^z(\vec{\boldsymbol{\sigma}}_i + \vec{\boldsymbol{\sigma}}_j) \cdot \boldsymbol{X}_{ij,-}^{(1)}$ |
| 2 | $\frac{1}{2}\lambda_s^1/\gamma_s$ | $\frac{4\pi}{M_N}\delta^3(\vec{\mathbf{r}})$ | $(\tau_i + \tau_j)^z(\vec{\boldsymbol{\sigma}}_i - \vec{\boldsymbol{\sigma}}_j) \cdot \boldsymbol{X}_{ij,+}^{(2)}$ |
| 3 | $\frac{1}{2\sqrt{6}}\lambda_s^2/\gamma_s$ | $\frac{4\pi}{M_N}\delta^3(\vec{\mathbf{r}})$ | $\mathcal{T}_{ij}(\vec{\boldsymbol{\sigma}}_i - \vec{\boldsymbol{\sigma}}_j) \cdot \boldsymbol{X}_{ij,+}^{(3)}$ |
| 4 | $a_t\lambda_t$ | $\frac{4\pi}{M_N}\delta^3(\vec{\mathbf{r}})$ | $(\vec{\boldsymbol{\sigma}}_i - \vec{\boldsymbol{\sigma}}_j)P_1 \cdot \boldsymbol{X}_{ij,+}^{(4)}$ |
| 5 | $\lambda_s^0/\gamma_s$ | $\frac{4\pi}{M_N}\delta^3(\vec{\mathbf{r}})$ | $(\vec{\boldsymbol{\sigma}}_i - \vec{\boldsymbol{\sigma}}_j)P_0 \cdot \boldsymbol{X}_{ij,+}^{(5)}$ |

In order to match the Girlanda formalism to the Danilov formalism we note the identity

$$\langle P|[-i\boldsymbol{\nabla}, \delta^3(\vec{\mathbf{r}})]|S\rangle = \langle P|\left\{-i\boldsymbol{\nabla}, \delta^3(\vec{\mathbf{r}})\right\}|S\rangle \tag{30}$$

which follows trivially since P waves are zero at the origin. Next we make use of the identical identities in spin and isospin space. (Note $P_0^\tau = \frac{1}{4}(1 - \vec{\boldsymbol{\tau}}_i \cdot \vec{\boldsymbol{\tau}}_j)$ and $P_1^\tau = \frac{1}{4}(3 + \vec{\boldsymbol{\tau}}_i \cdot \vec{\boldsymbol{\tau}}_j)$)

$$i(\vec{\boldsymbol{\sigma}}_i \times \vec{\boldsymbol{\sigma}}_j) = (\vec{\boldsymbol{\sigma}}_i - \vec{\boldsymbol{\sigma}}_j)(P_0 - P_1) \tag{31}$$

$$i(\vec{\boldsymbol{\tau}}_i \times \vec{\boldsymbol{\tau}}_j)^z = (\vec{\boldsymbol{\tau}}_i - \vec{\boldsymbol{\tau}}_j)^z(P_0^\tau - P_1^\tau) \tag{32}$$

The isospin operator $i(\vec{\boldsymbol{\tau}}_i \times \vec{\boldsymbol{\tau}}_j)^z$ only appears with the spin operator $(\vec{\boldsymbol{\sigma}}_i + \vec{\boldsymbol{\sigma}}_j)$ in the Girlanda potential. Since this spin operator only projects out the triplet state of the S wave, only the isosinglet part of the operator $i(\vec{\boldsymbol{\tau}}_i \times \vec{\boldsymbol{\tau}}_j)^z$ is projected out. Thus by Eq. (32) we find that in combination with the spin operator $(\vec{\boldsymbol{\sigma}}_i + \vec{\boldsymbol{\sigma}}_j)$ the isospin operator $i(\vec{\boldsymbol{\tau}}_i \times \vec{\boldsymbol{\tau}}_j)^z = (\vec{\boldsymbol{\tau}}_i - \vec{\boldsymbol{\tau}}_j)^z$. Finally using Eqs. (30), (31), and the fact that the identity $I$ is $I = P_0 + P_1$ one can straightforwardly match the Girlanda coefficients to the Danilov coefficients, giving the results shown in Table V. Also shown in Table V are the relation between the Zhu, Girlanda, Auxiliary, and Danilov formalisms. The primary goal in low energy hadronic parity-violation is to determine the value of the Danilov parameters. At low energies all of these different EFT formalisms can be shown to be equivalent to the Danilov parameters, as shown in Table V. Thus one can use whichever formalism is more convenient.

TABLE V: Translation between various formalisms of PV potential

| Zhu | Girlanda | Auxiliary | Danilov |
|---|---|---|---|
| $\frac{M_N(\frac{1}{a_t}-\mu)}{2\pi\Lambda_\chi^3}\left(C_1 - \tilde{C}_1 - 3(C_3 - \tilde{C}_3)\right)$ | $\frac{M_N(\frac{1}{a_t}-\mu)}{2\pi}\left(\mathcal{G}_1 - \tilde{\mathcal{G}}_1\right)$ | $-2\sqrt{2}g_1$ | $\lambda_t$ |
| $-\frac{M_N(\frac{1}{a_t}-\mu)}{\pi\Lambda_\chi^3}\left(2\tilde{C}_6 + (C_2 - C_4)\right)$ | $\frac{M_N(\frac{1}{a_t}-\mu)}{\pi}\mathcal{G}_6$ | $-4\sqrt{2}g_2$ | $\rho_t$ |
| $\frac{M_N(\gamma_s-\mu)}{2\pi\Lambda_\chi^3}\left(C_1 + \tilde{C}_1 + (C_3 + \tilde{C}_3)\right)$ | $\frac{M_N(\gamma_s-\mu)}{2\pi}\left(\tilde{\mathcal{G}}_1 + \mathcal{G}_1\right)$ | $-2\sqrt{2}g_3$ | $\lambda_s^0$ |
| $\frac{M_N(\gamma_s-\mu)}{2\pi\Lambda_\chi^3}\left(C_2 + C_4 + \tilde{C}_2 + \tilde{C}_4\right)$ | $\frac{M_N(\gamma_s-\mu)}{\pi}\mathcal{G}_2$ | $-2\sqrt{2}g_4$ | $\lambda_s^1$ |
| $-\frac{M_N(\gamma_s-\mu)\sqrt{6}}{\pi\Lambda_\chi^3}\left(C_5 + \tilde{C}_5\right)$ | $-\frac{M_N(\gamma_s-\mu)\sqrt{6}}{\pi}\mathcal{G}_5$ | $-4\sqrt{3}g_5$ | $\lambda_s^2$ |

Having matched the auxiliary coefficients $g_i$ to the Zhu coefficients we can now use the matching of the Zhu coefficients to the DDH "best" values to obtain estimates for the auxiliary coefficients which yields.

$$g_1 = -\frac{M_N(\frac{1}{a_t}-\mu)}{8\sqrt{2}\pi}\left[\frac{g_\omega\chi_\omega}{M_N m_\omega^2}h_\omega^0 - \frac{3g_\rho\chi_\rho}{M_N m_\rho^2}h_\rho^0\right] \sim 1.75\times10^{-10}\text{MeV}^{-1} \tag{33a}$$

$$g_2 = \frac{M_N(\frac{1}{a_t}-\mu)}{8\sqrt{2}\pi}\left[\frac{g_{\pi NN}}{\sqrt{2}M_N m_\pi^2}f_\pi + \frac{g_\rho}{M_N m_\rho^2}h_\rho^1 - \frac{g_\omega}{M_N m_\omega^2}h_\omega^1\right] \sim -6.34\times10^{-10}\text{MeV}^{-1} \tag{33b}$$

$$g_3 = \frac{M_N(\gamma_s-\mu)}{8\sqrt{2}\pi}\left[\frac{g_\omega(2+\chi_\omega)}{M_N m_\omega^2}h_\omega^0 + \frac{g_\rho(2+\chi_\rho)}{M_N m_\rho^2}h_\rho^0\right] \sim 1.50\times10^{-10}\text{MeV}^{-1} \tag{33c}$$

$$g_4 = \frac{M_N(\gamma_s-\mu)}{8\sqrt{2}\pi}\left[\frac{g_\rho(2+\chi_\rho)}{M_N m_\rho^2}h_\rho^1 + \frac{g_\omega(2+\chi_\omega)}{M_N m_\omega^2}h_\omega^1\right] \sim 1.47\times10^{-11}\text{MeV}^{-1} \tag{33d}$$

$$g_5 = \frac{M_N(\gamma_s-\mu)}{8\sqrt{2}\pi}\left[\frac{g_\rho(2+\chi_\rho)}{\sqrt{6}M_N m_\rho^2}h_\rho^2\right] \sim 4.39\times10^{-11}\text{MeV}^{-1} \tag{33e}$$

## V. Spin Observables

Having calculated the various PV amplitudes, we can now relate them to PV observables. One such observable is the neutron longitudinal asymmetry $A_N$[33]. In this case we scatter longitudinally polarized neutrons from an unpolarized deuteron target, and measure the difference of the two cross sections.

$$A_N = \frac{\sigma_+ - \sigma_-}{\sigma_+ + \sigma_-} \tag{34}$$

Here $\sigma_+$ ($\sigma_-$) represents the cross section of positive (negative) helicity neutrons.

In order to calculate observables, we need to write them in terms of the partial wave amplitudes calculated above. We denote the transition matrix by the operator $\mathbf{M}$. Of course, $\mathbf{M}$ is not diagonal in the orbital angular momentum basis, but rather is diagonal in terms of total angular momentum. Defining $M_{m_1',m_2';m_1,m_2}$ as the $T$ matrix where the neutron has initial (final) spin $m_2$, ($m_2'$), and the deuteron has initial (final) spin $m_1$, ($m_1'$),it can be shown

$$\begin{aligned} M_{m_1',m_2';m_1,m_2} =& \sqrt{4\pi}\sum_J\sum_{L,L'}\sum_{S,S'}\sum_{m_s,m_S'}\sum_{m_L'}\sqrt{2L+1}C^{Sm_S}_{1m_1,1/2m_2} \\ & C^{S'm_S'}_{1m_1',1/2m_2'}C^{JM}_{L0,Sm_S}C^{JM}_{L'm_L',S'm_S'}Y_{L'}^{m_L'}(\theta,\phi)M^J_{L'S',LS} \end{aligned} \tag{35}$$

Observables are most easily written in terms of this matrix $M_{m_1',m_2';m_1,m_2}$. Having Eq. (35), which gives $M_{m_1',m_2';m_1,m_2}$ in terms of the calculated functions $M^J_{L'S',LS}$, we can calculate

observables by truncating the sum over $J, L$, and $L'$ at some reasonable level. Thus the observable $A_N$ is given by

$$A_N = \frac{\sum\limits_{m_1',m_2'} \sum\limits_{m_1,m_2} (-1)^{1/2-m_2} \int d\Omega |M_{m_1',m_2';,m_2,m_2}|^2}{\sum\limits_{m_1',m_2'} \sum\limits_{m_1,m_2} \int d\Omega |M_{m_1',m_2';,m_2,m_2}|^2} \tag{36}$$

Explicitly summing over values of angular momentum from 0 to 1, and spin and $J$ from $J = {}^1\!/_2$ to $J = {}^3\!/_2$ we find.

$$\begin{aligned} A_N \cong & \frac{2}{3}\mathrm{Re}\left[\left(M^{1/2}_{0^1/_2,0^1/_2} + M^{1/2}_{1^1/_2,1^1/_2}\right)\left(M^{1/2}_{1^1/_2,0^1/_2}\right)^* + 2\sqrt{2}\left(M^{1/2}_{0^1/_2,0^1/_2} + M^{1/2}_{1^3/_2,1^3/_2}\right)\left(M^{1/2}_{1^3/_2,0^1/_2}\right)^*\right. \\ & \left. -4\left(M^{3/2}_{0^3/_2,0^3/_2} + M^{1/2}_{1^1/_2,1^1/_2}\right)\left(M^{3/2}_{1^1/_2,0^3/_2}\right)^* - 2\sqrt{5}\left(M^{3/2}_{0^3/_2,0^3/_2} + M^{3/2}_{1^3/_2,1^3/_2}\right)\left(M^{3/2}_{1^3/_2,0^3/_2}\right)^*\right] / \\ & \left[|M^{1/2}_{0^1/_2,0^1/_2}|^2 + 2|M^{3/2}_{0^3/_2,0^3/_2}|^2 + 3|M^{1/2}_{1^1/_2,1^1/_2}|^2 + 3|M^{3/2}_{1^3/_2,1^3/_2}|^2\right] \end{aligned} \tag{37}$$

By the optical theorem we note that $A_N$ can also be written as

$$\begin{aligned} A_N &= \frac{\sum_m \mathrm{Im}\left(M_{m,1/2;m,1/2}|_{\theta=0} - M_{m,-1/2;m,-1/2}|_{\theta=0}\right)}{\sum_m \mathrm{Im}\left(M_{m,1/2;m,1/2}|_{\theta=0} + M_{m,-1/2;m,-1/2}|_{\theta=0}\right)} \\ &\cong \frac{2}{3}\mathrm{Im}\left[M^{1/2}_{1^1/_2,0^1/_2} + 2\sqrt{2}M^{1/2}_{1^3/_2,0^1/_2} - 4M^{3/2}_{1^1/_2,0^3/_2} - 2\sqrt{5}M^{3/2}_{1^3/_2,0^1/_2}\right] / \\ &\quad \mathrm{Im}\left[M^{1/2}_{0^1/_2,0^1/_2} + 2M^{3/2}_{0^3/_2,0^3/_2} + 3M^{1/2}_{1^1/_2,1^1/_2} + 3M^{1/2}_{1^3/_2,1^3/_2}\right] \end{aligned} \tag{38}$$

Another PV observable is the spin rotation of the neutron as it passes through a deuteron target. In this experiment the neutron is transversely polarized and the rate of change of the rotation angle with respect to the distance traveled is[10, 33].

$$\frac{d\phi}{dz} = -\frac{4M_N N}{9k}\sum_m \mathrm{Re}\left[M_{m,1/2;m,1/2}|_{\theta=0} - M_{m,-1/2;m,-1/2}|_{\theta=0}\right] \tag{39}$$

where $N$ is the number of scattering centers per unit volume, and $k$ is the momentum of the neutron in the c.m. system. Using Eq. (35) we find

$$\frac{d\phi}{dz} = -\frac{4M_N N}{27k}\mathrm{Re}\left[M^{1/2}_{1^1/_2,0^1/_2} + 2\sqrt{2}M^{1/2}_{1^3/_2,0^1/_2} - 4M^{3/2}_{1^1/_2,0^3/_2} - 2\sqrt{5}M^{3/2}_{1^3/_2,0^3/_2}\right] \tag{40}$$

The final PV observable that we will consider is the deuteron target asymmetry. In this case an unpolarized beam of neutrons is scattered from a polarized deuteron target. At first the deuteron target is polarized in the positive $z$ direction, where $\hat{z}$ is the direction of the neutron's initial momentum. Then the neutron scatters off the deuteron target and we measure the cross section $\sigma_1$. In addition the deuteron target is polarized in the opposite direction and we measure the cross section $\sigma_{-1}$. If there is parity-violation one will find that $\sigma_1 \neq \sigma_{-1}$, and we define the target asymmetry as

$$A_D = \frac{\sigma_1 - \sigma_{-1}}{\sigma_1 + \sigma_{-1}} \tag{41}$$

$$\begin{aligned} A_D =& \frac{\sum\limits_{m_{1'},m_2'} \sum\limits_{m_2} \int d\Omega \left( |M_{m_1',m_2';1,m_2}|^2 - |M_{m_1',m_2';-1,m_2}|^2 \right)}{\sum\limits_{m_{1'},m_2'} \sum\limits_{m_2} \int d\Omega \left( |M_{m_1',m_2';1,m_2}|^2 + |M_{m_1',m_2';-1,m_2}|^2 \right)} \\ \cong& -\mathrm{Re}\left[ 2\left( M^{1/2}_{1^1/_2,1^1/_2} + M^{1/2}_{0^1/_2,0^1/_2} \right)\left( M^{1/2}_{1^1/_2,0^1/_2} \right)^* + \sqrt{2}\left( M^{1/2}_{1^3/_2,1^3/_2} + M^{1/2}_{0^1/_2,0^1/_2} \right)\left( M^{1/2}_{1^3/_2,0^1/_2} \right)^* \right. \\ & \left. -2\left( M^{3/2}_{1^1/_2,1^1/_2} + M^{3/2}_{0^3/_2,0^3/_2} \right)\left( M^{3/2}_{1^1/_2,0^3/_2} \right)^* + 2\sqrt{5}\left( M^{3/2}_{1^3/_2,1^3/_2} + M^{3/2}_{0^3/_2,0^3/_2} \right)\left( M^{3/2}_{1^3/_2,0^3/_2} \right)^* \right] / \\ & \left[ |M^{1/2}_{0^1/_2,0^1/_2}|^2 + 2|M_{0^3/_2,0^3/_2}|^2 + 3|M^{1/2}_{1^1/_2,1^1/_2}|^2 + 6|M^{1/2}_{1^3/_2,1^3/_2}|^2 \right] \end{aligned} \tag{42}$$

Again $A_D$ can also be calculated via the optical theorem.

$$\begin{aligned} A_D =& \frac{\sum_{m_2} \mathrm{Im}\left( M_{1,m_2;1,m_2}|_{\theta=0} - M_{-1,m_2;-1,m_2}|_{\theta=0} \right)}{\sum_{m_2} \mathrm{Im}\left( M_{1,m_2;1,m_2}|_{\theta=0} + M_{-1,m_2;-1,m_2}|_{\theta=0} \right)} \\ \cong& -\mathrm{Im}\left[ 2M^{1/2}_{1^1/_2,0^1/_2} + \sqrt{2}M^{1/2}_{1^3/_2,0^1/_2} - 2M^{3/2}_{1,1^1/_2,0^3/_2} + 2\sqrt{5}M^{3/2}_{1^3/_2,0^3/_2} \right] / \\ & \mathrm{Im}\left[ M^{1/2}_{0^1/_2,0^1/_2} + 2M^{3/2}_{0^3/_2,0^3/_2} + 3M^{1/2}_{1^1/_2,1^1/_2} + 6M^{1/2}_{1^3/_2,1^3/_2} \right] \end{aligned} \tag{43}$$

## VI. Results

Plotting our results for beam and target asymmetry as a function of center of mass energy, $E_{c.m}$, we find the plots given in Fig. 4. The thickness of the plot denotes the momentum cutoff variation, which runs from 200 MeV to 1500 MeV. It appears that the results begin to converge after 900 MeV as found by other authors[20]. Also it should be noted that the cutoff variation for the beam and target asymmetries at low energies is actually smaller than as shown in the plots, and is displayed with the given thickness in order that the plot be visible. The plots for the beam and target asymmetries extend all the way to 2.22 MeV,

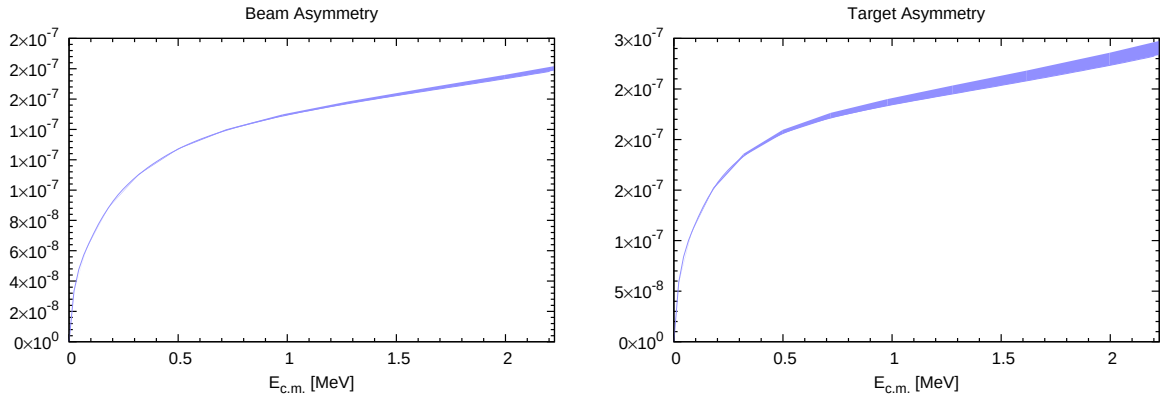


(a) (b)

FIG. 4: (Color online)Beam and target asymmetries as function of c.m. energy, $E_{c.m}$. Estimates for observables are found by using DDH "best" values. The right pane of the plot refers to the deuteron break-up energy

which is the deuteron breakup energy. However, the observables cannot be taken seriously at these high energies as higher partial waves and higher order contributions will become important. (It should also be noted that a significant difference was found at about .32 MeV if P waves were not included in the PC amplitudes.) The spin rotation observable had a value of $1.8 \times 10^{-8}$ rad cm$^{-1}$ with minimal cutoff variation on the order of .5% (We used a liquid deuterium number density of $N = .4 \times 10^{23}$atoms cm$^{-3}$[11].) This value is roughly two times the previous estimates for the spin rotation by Schiavilla et al.[10] and Song et al.[11]. Also the beam asymmetry has a value of $2.2 \times 10^{-8}$ with minimal cutoff variation, at $E_{lab} = 15$ keV, and again this is roughly a factor of two greater than previous calculations by Song et al.[11]. Finally the target asymmetry at $E_{lab} = 15$ keV has a value of $4.0 \times 10^{-8}$ again with minimal cutoff variation.

Finally in order to compare with possible experiments a table of all three observables in terms of their contributions from each of the $g_i$ is given below. The spin rotation is given at zero energy and the beam and target asymmetry are given at a lab energy of 15 keV. In order to obtain a prediction for the observable each row is multiplied by the appropriate value of $g_i$ and then these products are added together to yield the observable. Below are two tables with different values for the cutoff. The first table shows the cutoff at 200 MeV and the second at 1500 MeV.

TABLE VI: Values for observables at cutoff $\Lambda = 200$ MeV. In order to obtain the corresponding observable each number in a given column is multiplied by the appropriate $g_i$ and then all added together.

| $g_i$ | Rotation, $E_{lab} = 0$ keV | $A_N$, $E_{lab} = 15$ keV | $A_D$, $E_{lab} = 15$ keV |
|---|---|---|---|
| 1 | -18.7 rad cm$^{-1}$ MeV | -14.4 MeV | 8.92 MeV |
| 2 | -36.2 rad cm$^{-1}$ MeV | -39.6 MeV | -59.7 MeV |
| 3 | -10.2 rad cm$^{-1}$ MeV | -1.83 MeV | 1.65 MeV |
| 4 | 6.81 rad cm$^{-1}$ MeV | 1.22 MeV | -1.10 MeV |

TABLE VII: Values for observables at cutoff $\Lambda = 1500$ MeV. In order to obtain the corresponding observable each number in a given column is multiplied by the appropriate $g_i$ and then all added together.

| $g_i$ | Rotation, $E_{lab} = 0$ keV | $A_N$, $E_{lab} = 15$ keV | $A_D$, $E_{lab} = 15$ keV |
|---|---|---|---|
| 1 | -19.2 rad cm$^{-1}$ MeV | -14.5 MeV | 9.15 MeV |
| 2 | -38.0 rad cm$^{-1}$ MeV | -39.9 MeV | -59.8 MeV |
| 3 | -16.7 rad cm$^{-1}$ MeV | -2.71 MeV | 2.47 MeV |
| 4 | 11.1 rad cm$^{-1}$ MeV | 1.81 MeV | -1.65 MeV |

We can now compare our results for the spin rotation to previous calculations using a hyperspherical harmonics method or by solving a differential Faddeev equation in configuration space[10, 11]. Both of these papers calculated the numbers $I_n$ for the spin rotation which are defined by Eq. (44), where $c_n^{Gir}$ are defined in Table III. Using Tables V, VI, and VII it is straightforward to compute the values $I_n^{Gir}$ as predicted by pure EFT$_{\not\pi}$ at LO. The results from the two previous calculations via hybrid methods of the $nd$ spin rotation for the values $I_n^{Gir}$ [10, 11] are compared in Table VIII with those given by pure EFT$_{\not\pi}$ at LO as well as with EFT$_{\not\pi}$ at NLO which has been calculated in[12].

$$\frac{1}{N}\frac{d\phi}{dz} = \sum_{n=1}^{5} c_n^{Gir} I_n^{Gir} \tag{44}$$

TABLE VIII: This table compares the prediction for $I_n^{Gir}$ in Eq. (44) from the hybrid approaches of Schiavilla et al.[10] and Song et al.[11] to the EFT$_{\not\pi}$ LO predictions of this paper and NLO of Griesshammer et al.[12]. The variation in the values for EFT$_{\not\pi}$ approaches is due cutoff variation in the momentum integrals. For EFT$_{\not\pi}$-I, $\mu = 138$ MeV. Also $I_n^{Gir}$ is given in units of fm.

| $I_n^{\rm Gir}$ (fm) | EFT$_{\not\pi}$-I/AV18 | | EFT$_{\not\pi}$-I/AV18+UIX | | EFT$_{\not\pi}$ | |
|---|---|---|---|---|---|---|
| $n =$ | Song [11] | Schiavilla [10] | Song | Schiavilla | LO | NLO [12] |
| 1 | 61.6 | 65.6 | 60.0 | 63.2 | 129.3 - 135.7 | 98.5 - 120.3 |
| 2 | 60.6 | 62.3 | 58.8 | 57.8 | 35.0 - 57.1 | 33.4 - 51.9 |
| 4 | -76.1 | -77.9 | -75.7 | -75.2 | -59.6 - -77.2 | -48.2 - -67.2 |
| 5 | -9.46 | -9.89 | -6.62 | -6.12 | 7.16 - -8.66 | -1.85 - -10.6 |

The range of numbers given in Table VIII for EFT$_{\not\pi}$ at LO and NLO is simply due to cutoff variation in the numerical integration. Looking at the table we see that with the exception of the $n = 1$ term the EFT$_{\not\pi}$ approach within the cutoff variation gives results very similar to the hybrid approaches of Schiavilla et al. and Song et al.[10, 11]. However, at low cutoff values for the LO $n = 5$ term we see that it has a different sign than the other results. This is likely due to the fact that in EFT$_{\not\pi}$ this term is calculated by subtracting two terms one of which has a larger cutoff variation. We also note the $n = 2$ term for large cutoff values at LO clearly agrees with the hybrid schemes where three body forces are included[10, 11]. This should come as no surprise as the EFT$_{\not\pi}$ approach at LO necessarily includes a three-body force term. At larger values of cutoff it is clear the EFT$_{\not\pi}$ approach seems to converge towards the hybrid approaches. For LO EFT$_{\not\pi}$ the largest cutoff variation comes from the $g_3$ and $g_4$ terms, and the terms $n = 2$ through $n = 5$ all contain one of these terms, thus they have a much larger cutoff variation than the $n = 1$ term. The $n = 1$ term in the EFT$_{\not\pi}$ approaches is roughly a factor of two larger than in the hybrid approaches[10, 11].

This result is consistent with our spin rotation prediction of $1.8 \times 10^{-8}$ rad cm$^{-1}$ and beam asymmetry prediction of $2.2 \times 10^{-8}$ (see Fig. 4a) which were roughly a factor of two larger than the predictions given by the authors of the hybrid approaches [10, 11] in Table VIII. The NLO EFT$_{\not\pi}$ results do not seem to differ greatly from the LO predictions. However, the cutoff variation for the $n = 1$ term seems to be larger than that at LO.

Finally we should note that the calculation for the beam and target asymmetries were done using both the standard cross section methods and the optical theorem. Plotting the results from both, we found they were indistinguishable. This agreement confirms that our amplitudes are unitary and acts as a check on the validity of our results. For the values quoted in Tables VI and VII, it was found that for the beam and target asymmetries, the values from either the cross sections or optical theorem agreed to less than one percent.

Looking at our results we see from Tables VI and VII that the dominant contribution to all the observables comes from the $g_2$ term. The greatest contribution to this coefficient comes in particular from the quartet S to quartet P channel. Thus the observables are largely determined by the quartet S to quartet P part of the $g_2$ term. Also looking at the estimates of the $g_i$, Eqs. (33a) to (33e) , we see that $g_2$ is the only term that contains the one-pion exchange term from the DDH potential. Thus all of the observables are mostly given by one-pion exchange in agreement with previous findings[10, 11]. Finally we note that the target asymmetry is larger than the other two observables. Thus this could be a useful observable to find hadronic parity-violation. However, presumably a polarized target experiment would be more difficult than a polarized beam experiment.

## VII. Conclusion

Above we calculated the low energy PV $nd$ transition amplitudes using EFT$_{\not\pi}$. Matching the auxiliary field formalism onto the DDH potential, we made predictions for the coefficients of the auxiliary field formalism by using the DDH "best" values. Using these amplitudes and estimates for $g_i$, we were able to make predictions for the spin rotation, beam asymmetry, and target asymmetry in low energy $nd$ interactions. The values obtained for the neutron spin rotation and beam asymmetry were roughly a factor of two larger than those found by other authors using hybrid approaches[10, 11]. Unfortunately due to the smallness of these values they will still require very precise experiments. However, the DDH parameters used to predict the $g_i$ are neither theoretically or experimentally well determined, and therefore

the actual value for the observables given in this paper could differ by up to an order of magnitude from the predictions given here.

The largest contribution to parity-violation was shown to come from the coefficient $g_2$, which contains the one-pion exchange contribution, and such experiments should then allow one to determine its value. It is noted that to first order in parity-violation the $\Delta I = 2$ ($g_5$) term does not contribute. Thus $nd$ scattering is sensitive to four out of the five PV coefficients.

In principle we should be able to calculate to NLO in EFT$_{\not\pi}$ without the need for PV three-body forces[13]. Griesshammer, Schindler, and Springer calculated the NLO PV amplitudes using the partially resummed approach which introduces higher order contributions at NLO[12]. However, to calculate the NLO contributions without higher order terms, one must calculate the full off shell LO amplitude. Since a calculation of the full off shell LO amplitude is numerically expensive it will be left to a future publication.

# A. Appendix

In projecting out the amplitudes one has to perform angular integrations which are given by

$$\begin{aligned} U_{JL} =& \sqrt{\frac{4\pi}{3}} \int d\Omega_k \int d\Omega_p \frac{1}{a + \hat{\mathbf{k}} \cdot \hat{\mathbf{p}}} Y_{L'}^{m'_L\,*}(\hat{\mathbf{p}}) Y_L^{m_L}(\hat{\mathbf{k}}) \left( k Y_1^m(\hat{\mathbf{k}}) + 2p Y_1^m(\hat{\mathbf{p}}) \right) = \\ &= 4\pi \sqrt{\frac{2L+1}{2L'+1}} C^{L'0}_{L0,10} C^{L'm'_L}_{Lm_L,1m} (k Q_{L'}(a) + 2p Q_L(a)) \end{aligned} \tag{A.1}$$

where

$$Q_L = \frac{1}{2} \int_{-1}^{1} \frac{P_L(x)}{x + a} dx \tag{A.2}$$

are functions related to the Legendre polynomials of the second kind up to a factor of $(-1)^L$, and $P_L(x)$ are the standard Legendre polynomials.

The projection we must carry out is of the form

$$\boldsymbol{\mathcal{K}}(k,p)^J_{L'S',LS} = \int d\Omega_k \int d\Omega_p \left( \mathcal{Y}^M_{J,L'S'}(\hat{\mathbf{p}}) \right)^* \left( \boldsymbol{\mathcal{K}}^{ji} \right)^{\beta b}_{\alpha a} (\vec{\mathbf{k}}, \vec{\mathbf{p}}) \mathcal{Y}^M_{J,LS}(\hat{\mathbf{k}}) \tag{A.3}$$

(Note the polarization and spin indices are summed over corresponding indices that are not explicitly shown in the spin angle functions). Each matrix element of $\left( \boldsymbol{\mathcal{K}}^{ji} \right)^{\beta b}_{\alpha a} (\vec{\mathbf{k}}, \vec{\mathbf{p}})$ has a

different projection. Each of these four different projections has in turn four pieces given by Eqs. (12). Fortunately many of these terms can be related by time reversal simplifying the projection considerably. For simplicity we only show how to project out the first $g^{^3S_1-{}^3P_1}$ piece of the matrix element $\left[\left(\boldsymbol{\mathcal{K}}^{ji}\right)^{\beta b}_{\alpha a}(\vec{\mathbf{k}},\vec{\mathbf{p}})\right]_{11}$ as given in (14) and (12a), and simply quote the other results. In order to project this term out we use properties of spherical tensors and the Wigner-Eckart theorem to reduce the following expression to a sum over Clebsch-Gordan coefficients.

$$\begin{aligned} W_{JL} =& i\epsilon^{i\ell\kappa}\langle 1/2, m_2'|\sigma^\kappa\sigma^j|1/2, m_2\rangle(\vec{\mathbf{k}}+2\vec{\mathbf{p}})^\ell \\ =&\sqrt{\frac{2}{3}}\sum_{m,m'}\sum_{\kappa,q}\sqrt{2\kappa+1}C^{1m'}_{1m_1,1m}C^{1m'}_{1m_1',\kappa q}C^{1/2m_2'}_{1/2m_2,\kappa q}\langle 1/2||T_\kappa||1/2\rangle(-1)^m(\vec{\mathbf{k}}+2\vec{\mathbf{p}})^{-m} \end{aligned} \tag{A.4}$$

Using the above expression with (14),(12a), and (A.3) and, for the time being ignoring the isospin, we find the expression for our projection is.

$$\begin{aligned} V_{JL} =&\sqrt{\frac{4\pi}{3}}\frac{1}{kp}g^{^3S_1-{}^3P_1}\int d\Omega_p\int d\Omega_k\frac{1}{a+\hat{\mathbf{k}}\cdot\hat{\mathbf{p}}}\sum_{m_1,m_2}\sum_{m_L,m_S}\sum_{m_1',m_2'}\sum_{m_L',m_S'} \\ &C^{S'm_S'}_{1m_1',1/2m_2'}C^{Sm_S}_{1m_1,1/2m_2}C^{JM}_{Lm_L,Sm_S}C^{JM}_{L'm_L',S'm_S'} \\ &Y^{m_L'}_{L'}{}^*(\hat{\mathbf{p}})Y^{m_L}_L(\hat{\mathbf{k}})\left(kY_1^{-m}(\hat{\mathbf{k}})+2pY_1^{-m}(\hat{\mathbf{p}})\right)(-1)^m \\ &\sqrt{\frac{2}{3}}\sum_{m,m'}\sum_{\kappa,q}\sqrt{2\kappa+1}C^{1m'}_{1m_1,1m}C^{1m'}_{1m_1',\kappa q}C^{1/2m_2'}_{1/2m_2,\kappa q}\langle 1/2||T_\kappa||1/2\rangle \end{aligned} \tag{A.5}$$

Integration over the angular variable can be carried out trivially by using (A.1) leaving a sum of products of Clebsch-Gordan coefficients . Then using symmetry properties of the Clebsch-Gordan coefficients we find. (Note the bar notation is defined as $\bar{x}=2x+1$.)

$$\begin{aligned} V_{JL} =&8\pi g^{^3S_1-{}^3P_1}\sqrt{3}C^{L0}_{L'0,10}(-1)^{L-S-J}\frac{1}{kp}(kQ_{L'}(a)+2pQ_L(a))\times \\ &\times\sum_\kappa\sqrt{\bar{S}\bar{S}'\bar{L}'\bar{\kappa}}\langle 1/2||T_\kappa||1/2\rangle\left\{\begin{array}{ccc} 1/2 & \kappa & 1/2 \\ 1 & S' & 1\end{array}\right\}\left\{\begin{array}{ccc} 1 & 1 & 1 \\ 1/2 & S' & S\end{array}\right\}\left\{\begin{array}{ccc} L' & 1 & L \\ S & J & S'\end{array}\right\} \end{aligned} \tag{A.6}$$

in terms of 6-j symbols[34]. The sum over $\kappa$ can be removed by use of the identity[35].

$$\sum_\kappa\bar{\kappa}\left\{\begin{array}{ccc} 1/2 & \kappa & 1/2 \\ 1 & S' & 1\end{array}\right\}\left\{\begin{array}{ccc} 1/2 & 1/2 & \kappa \\ 1 & 1 & j\end{array}\right\}=\delta_{S'j}\frac{1}{\bar{S}'} \tag{A.7}$$

yielding

$$V_{JL} = 8\pi g^{{}^3S_1-{}^3P_1}\sqrt{6}C^{L0}_{L'0,10}(-1)^{L-S-J}\sqrt{\bar{S}\bar{S}'\bar{L}'}\left(\frac{1}{2}\delta_{S'1/2}+\delta_{S'3/2}\right)\times \\ \times\begin{Bmatrix} 1 & 1 & 1 \\ 1/2 & S' & S\end{Bmatrix}\begin{Bmatrix} L' & 1 & L \\ S & J & S'\end{Bmatrix}\frac{1}{kp}(kQ_{L'}(a)+2pQ_L(a)) \tag{A.8}$$

Using time reversal invariance and including our coefficients, as well as the isospin projection, we find the projection for the $\left[\boldsymbol{\mathcal{K}}(k,p)^J_{L'S',LS}\right]_{11}$ term is

$$-y_d g^{{}^3S_1-{}^1P_1}4\pi\sqrt{3}(-1)^{3/2+2S+L-J}\delta_{S'1/2}\sqrt{\bar{S}\bar{L}}C^{L'0}_{L0,10}\begin{Bmatrix} 1/2 & 1 & S \\ L & J & L'\end{Bmatrix}\frac{1}{kp}(kQ_{L'}(a)+2pQ_L(a)) \tag{A.9}$$

$$-y_d g^{{}^3S_1-{}^1P_1}4\pi\sqrt{3}(-1)^{3/2+2S'+L'-J}\delta_{S1/2}\sqrt{\bar{S}'\bar{L}'}C^{L0}_{L'0,10}\begin{Bmatrix} 1/2 & 1 & S' \\ L' & J & L\end{Bmatrix}\frac{1}{kp}(2kQ_{L'}(a)+pQ_L(a))$$

$$-y_d g^{{}^3S_1-{}^3P_1}8\pi\sqrt{6}C^{L0}_{L'0,10}(-1)^{L-S-J}\sqrt{\bar{S}\bar{S}'\bar{L}'}\left(\frac{1}{2}\delta_{S'1/2}+\delta_{S'3/2}\right)\begin{Bmatrix} 1 & 1 & 1 \\ 1/2 & S' & S\end{Bmatrix}\begin{Bmatrix} L' & 1 & L \\ S & J & S'\end{Bmatrix}\times$$

$$\times\frac{1}{kp}(kQ_{L'}(a)+2pQ_L(a))$$

$$-y_d g^{{}^3S_1-{}^3P_1}8\pi\sqrt{6}C^{L'0}_{L0,10}(-1)^{L'-S'-J}\sqrt{\bar{S}\bar{S}'\bar{L}}\left(\frac{1}{2}\delta_{S1/2}+\delta_{S3/2}\right)\begin{Bmatrix} 1 & 1 & 1 \\ 1/2 & S & S'\end{Bmatrix}\begin{Bmatrix} L & 1 & L' \\ S' & J & S\end{Bmatrix}\times$$

$$\times\frac{1}{kp}(2kQ_{L'}(a)+pQ_L(a))$$

Now combining isospin with our spin projections we find the $\left[\boldsymbol{\mathcal{K}}(k,p)^J_{L'S',LS}\right]_{12}$ term projected out is

$$
\begin{aligned}
&- 8\pi\sqrt{3}(-1)^{1+S'+L-J}\delta_{S1/2}y_t\left(\frac{2}{3}g^{^1S_0-^3P_0}_{(\Delta I=1)}-g^{^1S_0-^3P_0}_{(\Delta I=0)}\right)\times \qquad (A.10)\\
&\times C^{L0}_{L'0,10}\sqrt{\bar{L}'\bar{S}'}\left(\frac{1}{2}\delta_{S'1/2}+\delta_{S'3/2}\right)\left\{\begin{array}{ccc} L' & 1 & L\\ S & J & S'\end{array}\right\}\frac{1}{kp}(kQ_{L'}(a)+2pQ_L(a))\\
&- y_t g^{^3S_1-^1P_1}4\pi\sqrt{3}(-1)^{1/2+2S'+L-J}\delta_{S1/2}\sqrt{\bar{L}'\bar{S}'}C^{L0}_{L'0,10}\left\{\begin{array}{ccc} L' & 1 & L\\ S & J & S'\end{array}\right\}\frac{1}{kp}\left(2kQ_{L'}(a)+pQ_L(a)\right)\\
&+ y_t g^{^3S_1-^3P_1}24\pi\frac{1}{\sqrt{3}}(-1)^{S'-L-J}\delta_{S1/2}\sqrt{\bar{S}'\bar{L}'}C^{L0}_{L'0,10}\left\{\begin{array}{ccc} 1 & 1 & 1\\ 1/2 & S' & 1/2\end{array}\right\}\left\{\begin{array}{ccc} L' & 1 & L\\ S & J & S'\end{array}\right\}\frac{1}{kp}(2kQ_{L'}(a)+pQ_L(a))
\end{aligned}
$$

Now using time reversal symmetry we see the projection of the $\left[\boldsymbol{\mathcal{K}}(k,p)^J_{L'S',LS}\right]_{21}$ term is

$$
\begin{aligned}
&- 8\pi\sqrt{3}(-1)^{1+S+L'-J}\delta_{S'1/2}y_t\left(\frac{2}{3}g^{^1S_0-^3P_0}_{(\Delta I=1)}-g^{^1S_0-^3P_0}_{(\Delta I=0)}\right)\times \qquad (A.11)\\
&\times C^{L'0}_{L0,10}\sqrt{\bar{L}\bar{S}}\left(\frac{1}{2}\delta_{S1/2}+\delta_{S3/2}\right)\left\{\begin{array}{ccc} L & 1 & L'\\ S' & J & S\end{array}\right\}\frac{1}{kp}(2kQ_{L'}(a)+pQ_L(a))\\
&- y_t g^{^3S_1-^1P_1}4\pi\sqrt{3}(-1)^{1/2+2S+L'-J}\delta_{S'1/2}\sqrt{\bar{L}\bar{S}}C^{L'0}_{L0,10}\left\{\begin{array}{ccc} L & 1 & L'\\ S' & J & S\end{array}\right\}\frac{1}{kp}\left(kQ_{L'}(a)+2pQ_L(a)\right)\\
&+ y_t g^{^3S_1-^3P_1}24\pi\frac{1}{\sqrt{3}}(-1)^{S-L'-J}\delta_{S'1/2}\sqrt{\bar{S}\bar{L}}C^{L'0}_{L0,10}\left\{\begin{array}{ccc} 1 & 1 & 1\\ 1/2 & S & 1/2\end{array}\right\}\left\{\begin{array}{ccc} L & 1 & L'\\ S' & J & S\end{array}\right\}\frac{1}{kp}(kQ_{L'}(a)+2pQ_L(a))
\end{aligned}
$$

Now combining the spin with the isospin projections we find the projection of the $\left[\boldsymbol{\mathcal{K}}(k,p)^J_{L'S',LS}\right]_{22}$ term is

$$
\begin{aligned}
&-y_t g^{^1S_0-^3P_0}_{(\Delta I=0)}12\pi\sqrt{6}(-1)^{1/2-L-J}\delta_{S'1/2}\delta_{S1/2}\sqrt{\bar{L}'}C^{L0}_{L'0,10}\left\{\begin{array}{ccc} L' & 1 & L\\ S & J & S'\end{array}\right\}\frac{1}{kp}(kQ_{L'}(a)+pQ_L(a))\\
&\qquad (A.12)\\
&+y_t g^{^1S_0-^3P_0}_{(\Delta I=1)}8\pi\sqrt{6}(-1)^{1/2-L-J}\delta_{S'1/2}\delta_{S1/2}\sqrt{\bar{L}'}C^{L0}_{L'0,10}\left\{\begin{array}{ccc} L' & 1 & L\\ S & J & S'\end{array}\right\}\frac{1}{kp}(kQ_{L'}(a)+pQ_L(a))
\end{aligned}
$$

## Acknowledgments

I would like to thank Harald W. Griesshammer, L. Girlanda, and Matthias Schindler for useful discussions, Barry R. Holstein for guidance during this project, and U. van Kolck for useful input. This work is supported in part by the National Science Foundation under Grant No. NSF-PHY 0855119

---

[1] B. Desplanques, J. F. Donoghue, and B. R. Holstein, Ann. Phys. **124**, 449 (1980).

[2] B. R. Holstein, Nucl. Phys. **A844**, 160c (2010).

[3] S.-L. Zhu, C. M. Maekawa, B. R. Holstein, M. J. Ramsey-Musolf, and U. van Kolck, Nucl. Phys. **A748**, 435 (2005).

[4] S. R. Beane, P. F. Bedaque, W. C. Haxton, D. R. Phillips, and M. J. Savage (2000).

[5] G. Danilov, Phys. Lett. **18**, 40 (1965).

[6] L. Girlanda, Phys.Rev. **C77**, 067001 (2008).

[7] D. R. Phillips, M. R. Schindler, and R. P. Springer, Nucl. Phys. **A822**, 1 (2009).

[8] M. R. Schindler and R. P. Springer, Nucl. Phys. **A846**, 51 (2010).

[9] J. W. Shin, S. Ando, and C. H. Hyun, Phys.Rev. **C81**, 055501 (2010).

[10] R. Schiavilla, M. Viviani, L. Girlanda, A. Kievsky, and L. E. Marcucci, Phys.Rev. **C78**, 014002 (2008). [Erratum. Phys. Rev. C **83**, 029902(E) (2011).]

[11] Y.-H. Song, R. Lazauskas, and V. Gudkov, Phys.Rev. **C83**, 015501 (2011).

[12] H. W. Griesshammer, M. R. Schindler, and R. P. Springer, Eur.Phys.J. **A48**, 7 (2012).

[13] H. W. Griesshammer and M. R. Schindler, Eur. Phys. J. **A46**, 73 (2010).

[14] F. Gabbiani, P. F. Bedaque, and H. W. Griesshammer, Nucl. Phys. **A675**, 601 (2000).

[15] P. F. Bedaque and H. W. Griesshammer, Nucl. Phys. **A671**, 357 (2000).

[16] D. B. Kaplan, Nucl.Phys. **B494**, 471 (1997).

[17] D. B. Kaplan, M. J. Savage, and M. B. Wise, Phys. Lett. **B424**, 390 (1998).

[18] P. F. Bedaque, G. Rupak, H. W. Griesshammer, and H.-W. Hammer, Nucl. Phys. **A714**, 589 (2003).

[19] V. Gudkov and Y.-H. Song, Phys.Rev. **C82**, 028502 (2010).

[20] H. W. Griesshammer, Nucl. Phys. **A744**, 192 (2004).

[21] P. F. Bedaque, H. W. Hammer, and U. van Kolck, Phys.Rev.Lett. **82**, 463 (1999).

[22] P. F. Bedaque, H. Hammer, and U. van Kolck, Nucl.Phys. **A646**, 444 (1999).

[23] P. F. Bedaque, H. Hammer, and U. van Kolck, Nucl.Phys. **A676**, 357 (2000).

[24] J. H. Hetherington and L. H. Schick, Phys. Rev. **137**, B935 (1965).

[25] R. Cahill and I. Sloan, Nucl. Phys. **A165**, 161 (1971).

[26] R. Aaron and R. D. Amado, Phys. Rev. **150**, 857 (1966).

[27] E. Schmid and H. Ziegelmann, *The Qauntum Mechanical Three-Body Problem, Vieweg Tract in Pure and Applied Physics Vol. 2* (Pergamon Press, 1974).

[28] G. Barton, Nuovo Cim. **19**, 512 (1961).

[29] V. M. Dubovik and S. V. Zenkin, Annals Phys. **172**, 100 (1986).

[30] G. B. Feldman, G. A. Crawford, J. Dubach, and B. R. Holstein, Phys. Rev. **C43**, 863 (1991).

[31] A. Manohar and H. Georgi, Nucl.Phys. **B234**, 189 (1984).

[32] J. F. Donoghue, E. Golowich, and B. R. Holstein, Phys. Rev. D **30**, 587 (1984).

[33] R. Schiavilla, J. Carlson, and M. W. Paris, Phys. Rev. **C70**, 044007 (2004).

[34] G. Strobel, Nucl.Phys. **A96**, 229 (1967).

[35] A. Edmonds, *Angular Momentum In Qauntum Mechanics* (Princeton University Press, 1960).